Green Chemistry

CRITICAL REVIEW

View Article Online
View Journal | View Issue

Cite this: *Green Chem.*, 2025, **27**, 14744

Harnessing germanium from industrial residues and electronic waste for a sustainable energy future

Rajiv Ranjan Srivastava[a,b] and Sadia Ilyas *[a,b]

Traditionally, germanium has been a critical dopant in the silica core of fiber optics, facilitating high-speed internet and data transfer, and functions as a semiconductor in N-type diodes. Over the past decade, its importance has greatly expanded to multi-junction solar cells, where it serves as a substrate, providing a foundation for other semiconductor layers. Despite rising demands from renewable energy and semiconductor industries, germanium has no primary ores and is found only as a companion element with others. It is primarily sourced as a by-product from industrial residues like zinc refinery residues (ZRR) and coal burnt fly-ash (CFA), with concentrations ranging between 0.04–0.5% and 0.05–1.7%, respectively. Given the scarcity of germanium, its recovery through recycling of electronic waste is also gaining interest. However, the recovery process from both primary and secondary sources is complex, involving several key steps to ensure efficient extraction. Therefore, a comprehensive understanding of these processes, along with thermodynamic strategies applied to different materials, is essential. Consequently, this review covers germanium recovery from major primary and secondary resources, involving leaching, solvent extraction, ion exchange, and precipitation methods, with a focus on the underlying thermodynamics. Additionally, the environmental impacts of different extraction schemes are assessed using life-cycle analysis, revealing the global warming potential (GWP) of 852 kg CO_2-eq for ZRR and 698 kg CO_2-eq for CFA. In contrast, recycled germanium exhibits a much lower GWP of 163 kg CO_2-eq, highlighting the importance of recycling efforts in advancing Sustainable Development Goals 7, 12, and 13.

Received 14th June 2025,
Accepted 16th October 2025

DOI: 10.1039/d5gc03018h

rsc.li/greenchem

Green foundation

1. We explore the resource recovery of germanium, a critical raw material essential for sustainable energy technologies such as solar cells and semiconductors. The focus is on processing the industrial residues from zinc refineries, coal-fired power plants, and electronic waste. The study therefore aligns with the United Nations Sustainable Development Goals 7 (affordable and clean energy), 12 (responsible consumption and production), and 13 (climate action).

2. The strategies presented for efficient germanium recovery from by-products and waste materials align with green chemistry principles by reducing dependency on primary resources and minimizing environmental impacts. Key advancements in mass transfer techniques—solid–liquid, liquid–liquid, and liquid–solid—are also discussed within this context. Moreover, a comparative life-cycle assessment demonstrates that recycling electronic waste significantly reduces environmental burdens, with a notable decrease in global warming potential to 163 kg CO_2-equivalent.

3. A detailed long-term sustainability model for germanium supply is discussed along with the static flows and stocks of germanium, emphasizing improved recycling practices to ensure a reliable supply for renewable energy applications. This model supports the transition to a low-carbon economy by promoting resource efficiency and circularity of critical raw materials.

1. Introduction

Germanium (Ge), which belongs to Group IVA in the periodic table, is an important semimetal or metalloid that exhibits both metallic and non-metallic properties.[1,2] Due to the intrinsic properties of semi-conductivity, doping Ge with other elements like arsenic, gallium, and indium has enabled its extensive applications in electronics mainly as a key component in diodes.[3,4] Although silicon has largely replaced germanium in electronics,

[a]*Process Metallurgy, Minerals and Metallurgical Engineering Division, Department of Civil, Environmental and Natural Resources Engineering, Luleå University of Technology, Luleå 97187, Sweden. E-mail: sadia.ilyas@ltu.se*
[b]*Wallenberg Initiative Materials Science for Sustainability (WISE), Department of Civil, Environmental and Natural Resources Engineering, Luleå University of Technology, Luleå 97187, Sweden*

its higher refractive index (*i.e.*, 4.0026 at 11 μm), coupled with excellent long wavelength transmission in the infrared (18–23 μm) and high resistivity (2.3×10^8 Ω cm), has led to major applications (as $GeCl_4$) in optical fibers and wide-angle lenses for cameras and microscopes.[5–8] The wide array of germanium usages is illustrated in Fig. 1a, while Table 1 highlights its key roles in advanced renewable energy applications.

Germanium is a key enabler of sustainable energy technologies, both as a performance-enhancing dopant and as a functional material in high-efficiency energy systems. One of the most prominent applications is in multi-junction photovoltaic (PV) cells,[9,10] in particular the PV cells used in space-based solar power systems and terrestrial concentrator photovoltaics, where it often serves as the bottom substrate layer due to its compatible lattice constant and superior electron mobility.[11,12] These advanced PVs can achieve conversion efficiencies exceeding 40%, far surpassing traditional silicon-based panels, and are central to the long-term adoption of high-efficiency, low-emission renewable energy technologies.[9–12] Additionally, germanium's role is also rapidly expanding in thin-film PV technologies, especially in amorphous silicon–germanium (a-SiGe) tandem cells, offering flexible, light weight, and cost-effective alternatives for portable energy systems.[13,14]

In the field of energy-efficient communication infrastructure, germanium is a core constituent of fiber-optic technologies.[5–8] Its most commercially significant derivative, germanium tetrachloride ($GeCl_4$), is used in doping silica to form the refractive core of optical fibers. These fibers enable the high-speed transmission of data with minimal loss, forming the backbone of modern internet and telecommunication networks. The growth in the integration of smart grids, decentralized renewable energy systems, and remote digital control platforms further accelerates demand for such infrastructure. With the global expansion of data centers, 5G networks, and the Internet of Things (IoT), the consumption of optical fibers and consequently $GeCl_4$ is projected to increase nearly eightfold by 2030.[15] Thus, germanium plays an indirect yet essential role in improving energy efficiency through next-generation communication technologies.

Despite this wide array of applications, germanium faces a profound and worsening supply–demand imbalance, driven by increasing consumption in both traditional and emerging technologies. Germanium's average crustal abundance is only 1.3 to 1.6 ppm,[16] making it one of the rarer technological elements. It is almost absent in independent mineral deposits,[17] and it mainly co-exists with zinc sulfide ore (*i.e.*, sphalerite),[18] which accounts for about 1/3rd of the global recoverable quantity of germanium (*i.e.*, ~38 kt).[19] Currently, about 100 t per annum of germanium is sourced from refining residues,[20] while the remaining demand is met by coal fly ash with a

Rajiv Ranjan Srivastava

Rajiv R. Srivastava is a Postdoctoral Fellow with the Wallenberg Initiative Materials Science for Sustainability—WISE and in Process Metallurgy at the Department of Civil, Environmental and Natural Resources Engineering, Luleå University of Technology, Sweden. His major research is related to sustainable hydrometallurgy of energy-critical and strategic elements. With extensive experience bridging academic research and industrial scale-up, he specializes in leaching, solvent extraction, precipitation, and electrowinning of critical and rare earth metals. He actively contributes to several journals, while authored more than 50 scientific papers, holds 6 patents, edited 4 books, and wrote numerous book chapters, alongside some of his developed technologies are successfully implemented in metal recycling industries.

Sadia Ilyas

Sadia Ilyas is an Associate Professor, and the Wallenberg Initiative Materials Science for Sustainability—WISE Fellow for 'Sustainable and Efficient Metal Recovery in a Circular Economy' at the Department of Civil, Environmental and Natural Resources Engineering, Luleå University of Technology, Sweden. Her research primarily focuses on low-emission hydrometallurgical processes and innovative technologies for the extraction and recycling of critical and strategic metals from both primary and secondary resources. She is an expert in the UN-Sustainable Development Goals, Green Deal initiatives, and life-cycle analysis related to critical metals production and related value chains. She also serves on the editorial boards of Toxicological & Environmental Chemistry, Communications Earth & Environment, Frontiers in Bioengineering and Biotechnology, Journal of Sustainable Metallurgy, PLOS ONE, and Journal of Microbiology-MIKROBIOLOGIJA, in different capacities. With over 15 years of international academic experience, she has led numerous national and international research projects. Throughout her career, she has published more than 100 scientific articles, edited six books, and holds nine patents for technical inventions, three of which have been successfully transferred to industry.

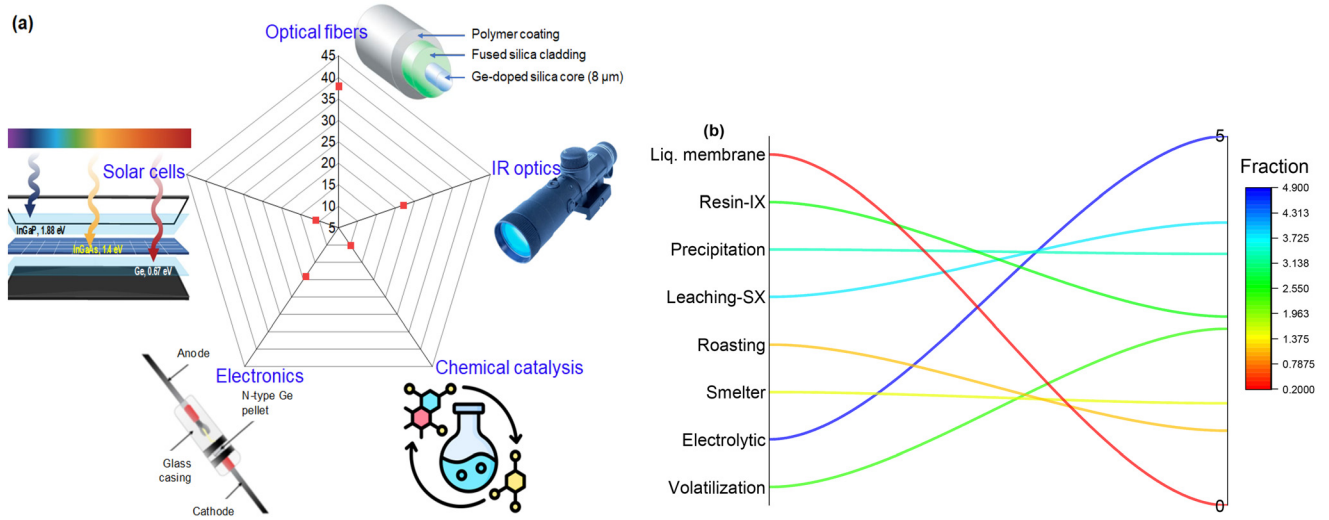

Fig. 1 [a] Representation of germanium's key role in major sectors. [b] Fraction of scientific literature discussing Ge extraction using pyrometallurgical and hydrometallurgical operations over the last two decades.

Table 1 Overview of application areas where Ge plays a crucial role in advancing renewable and sustainable energy solutions

Application in renewable energy	Description of the key role of germanium
Photovoltaic (PV) cells	Germanium is a crucial material in the development of high-efficiency PV (solar) cells. It is commonly used as the base substrate, which is more efficient than traditional silicon-based cells. These advanced solar cells are particularly important in space applications and for concentrated solar power systems.
Multi-junction solar cells	In addition to its use in single-junction PV cells, germanium is widely used in multi-junction solar cells, which can convert sunlight into electricity more efficiently by stacking multiple layers of different materials, each optimized to absorb different wavelengths of light. This technology is essential in reaching high efficiency levels needed for sustainable energy generation, particularly in solar power.
Light emitting diodes (LEDs) and optoelectronics	Germanium is used in optoelectronic devices such as LEDs, lasers, and photodetectors, which are important components in various renewable energy systems, such as solar energy harvesters and light-based communication systems. LEDs are energy-efficient lighting solutions that reduce electricity consumption, making them a sustainable alternative to traditional incandescent and fluorescent bulbs. Furthermore, the use of germanium in optoelectronics helps improve energy efficiency in electronic devices, which is crucial for overall energy conservation.
Energy-efficient electronics	Germanium is also employed in the electronics used in renewable energy systems. For example, in devices that regulate the flow of electricity from renewable sources (like wind turbines and solar panels), Ge-based semiconductors can improve the energy efficiency and performance of these systems. Low power consumption and high speed make them ideal for smart grids, energy management, and other sustainable energy applications.
Carbon footprint reduction	Although germanium extraction can have environmental impacts, its role in improving the efficiency of renewable energy technologies indirectly contributes to reducing the carbon footprint. More efficient solar panels, LEDs, and electronics that use germanium require less material and energy to operate, reducing the overall environmental impact compared to less efficient technologies.

small contribution derived from the recycling of waste materials.[21] Additionally, germanium reserves are also geopolitically concentrated, creating vulnerabilities in international supply chains. China alone holds 41% of global germanium reserves, while Russia controls nearly 10% of the world's reserves. In contrast, Europe has virtually no significant domestic reserves and is heavily reliant on imports. This limited supply, coupled with a low recycling rate, results in the growing disparity between supply and demand due to the current supply risk of 8.1 out of 10.[1] Consequently, germanium has been designated as a critical metal by both the United States, which lists it among 50 essential commodities,[22] and the European Union's new list of 34 critical raw minerals.[23] In response, the European Critical Raw Materials Act has set a 2030 target that at least 15% of the EU's annual germanium consumption be met through domestic recycling, a considerable increase from the current 2% recycling level.[24,25]

Against this backdrop of rising demand and constrained supply, efforts to enhance germanium recovery from both industrial residues and electronic waste have become increasingly important. Currently, the extraction of germanium is performed using both pyrometallurgical and hydrometallurgical techniques.[26] The pyrometallurgical operations rely on differences in boiling points and typically involve processes like smelting, sintering, and high-temperature gas-phase reactions.[27–29] Hydrometallurgical techniques, on the other

hand, depend on factors such as metal solubility, ionic radius, charge density, reduction potential, and favorable pH. In hydrometallurgical extraction, Ge-bearing materials are often subjected to leaching with mineral acids or alkaline solutions. Subsequently, to isolate germanium from the complex multi-metal-leached solutions, various separation steps are employed, such as tannin precipitation,[30] ferric hydroxide precipitation,[31] organic precipitation,[32] ion exchange,[33] and solvent extraction.[34–36] Fig. 1b presents a bibliometric analysis of research over the past two decades, clearly indicating a shift from pyrometallurgical to hydrometallurgical approaches. Despite this transition, volatilization studies remain prominent, as this step, though technically challenging, is often essential for mobilizing germanium from industrial residues, enabling subsequent hydrometallurgical processing. The decline in roasting-related research can be attributed to the established zinc extraction processes, where zinc is the primary target and Ge is a secondary by-product. In contrast, the growth in hydrometallurgical studies is largely driven by its lower energy requirements, reduced CO_2 and SO_2 emissions, and its effectiveness for low-grade and polymetallic feedstocks, where Ge often occurs in trace amounts. Recent advances in separation and purification technologies, such as solvent extraction, have further increased interest in hydrometallurgy. The notable surge in hydrometallurgical research post-2015 coincides with the Paris Climate Agreement, highlighting a broader move towards more sustainable extraction technologies.

Although germanium is typically recovered in small quantities, it remains critical and irreplaceable in a range of cutting-edge technologies, including fiber optics, solar cells, and semiconductors.[37] Therefore, a comprehensive understanding of Ge-extraction processes is crucial, not only to enhance the efficiency of current recovery methods but also to unlock newly identified resource streams like marine ore crusts in the Sea of Japan (up to 96 ppm Ge)[38] and coal seams in the Donetsk Basin (up to 63 ppm Ge).[39] Despite growing interest, recent review articles fall short of providing a holistic perspective on germanium extraction, often due to their reginal focus,[15,19] limited descriptive discussion of leaching processes,[26] inaccuracies in solution chemistry,[15,40,41] insufficient coverage of extraction thermodynamics,[42] and limited attention to coal-based resources.[43] Henceforth, this review aims to fill these gaps by providing a detailed exploration of all aspects of germanium harnessing. Furthermore, it includes a vital discussion on environmental impacts of extraction methods, with life-cycle assessments (LCA) and economic analyses of processes, involving zinc refinery residues (ZRR), coal burning residue (CBR), and electronic (e-)waste.

The review begins by addressing the thermodynamic challenges associated with Ge extraction, including thermal behavior, phase stability of its compounds, aqueous speciation, and dissolution properties. These are critical factors for understanding the chemical behavior of germanium. Building on this foundation, the review then explores extraction and recovery methods across diverse feedstocks, alongside separation techniques such as solvent and solid-phase extraction. Moving from process-level considerations to system-level implications, the review evaluates the environmental and energy performance through LCA. This serves as a basis for developing long-term sustainability models that incorporate circular economy principles and recycling of waste materials. Furthermore, the key findings are summarized, and future research directions are proposed based on the insights gained throughout this review. Overall, this review is framed within the broader context of the United Nations Sustainable Development Goals (UN-SDGs).[44] Specifically, these are: Goal 7, which focuses on enhancing energy efficiency; Goal 12, which focuses on responsible use and circular material flows with waste minimization; and Goal 13, which promotes mitigation of environmental impacts through sustainable resource management. By integrating technological, environmental, and economic perspectives, this review highlights the essential role of urban mining and recycling innovations in advancing both resource resilience and climate objectives.

2. Thermodynamic challenges and considerations in germanium extraction

The thermodynamic behavior of germanium and its compounds plays a central role in determining the efficiency, selectivity, and environmental sustainability of extraction processes. Therefore, the key thermodynamic factors governing Ge extraction from major industrial residues, with particular attention given to volatility, phase transformations, solubility, and aqueous speciation, are discussed with the aim to identify areas where optimization could significantly enhance process efficiency.

2.1. Ge-migration from sphalerite mineral

In naturally occurring zinc-bearing ores (mainly sphalerite), Ge primarily occurs in trace amounts as a companion metal. The sphalerite is typically subjected to roasting at 800–850 °C to convert ZnS → ZnO prior to neutral leaching in diluted sulfuric acid. Germanium, being a thiophilic element, has a strong affinity toward sulfur and tends to form sulfides such as GeS and GeS_2. However, the Ge–S phase diagram (Fig. 2a) indicates that at this temperature, the probability of GeS_2 remaining in the roasted mass is negligible. It neither liquefies nor persists in the roasted residue,[45] suggesting that most of the germanium either remains in a solid oxidized form (*i.e.*, GeO_2) or volatilizes partially as $GeO_{(g)}$, depending on redox conditions. This reveals the need for improved control of oxygen availability during the roasting process.

2.2. Thermal evolution and Ge migration in coal combustion

In contrast to sphalerite, only 1% of the total germanium mined with coal can be transformed into refined product.[46] The combustion of coal presents a more complex thermodynamic environment for germanium behavior. Germanium in lignite is often bound to organic matter *via* strong Ge–O

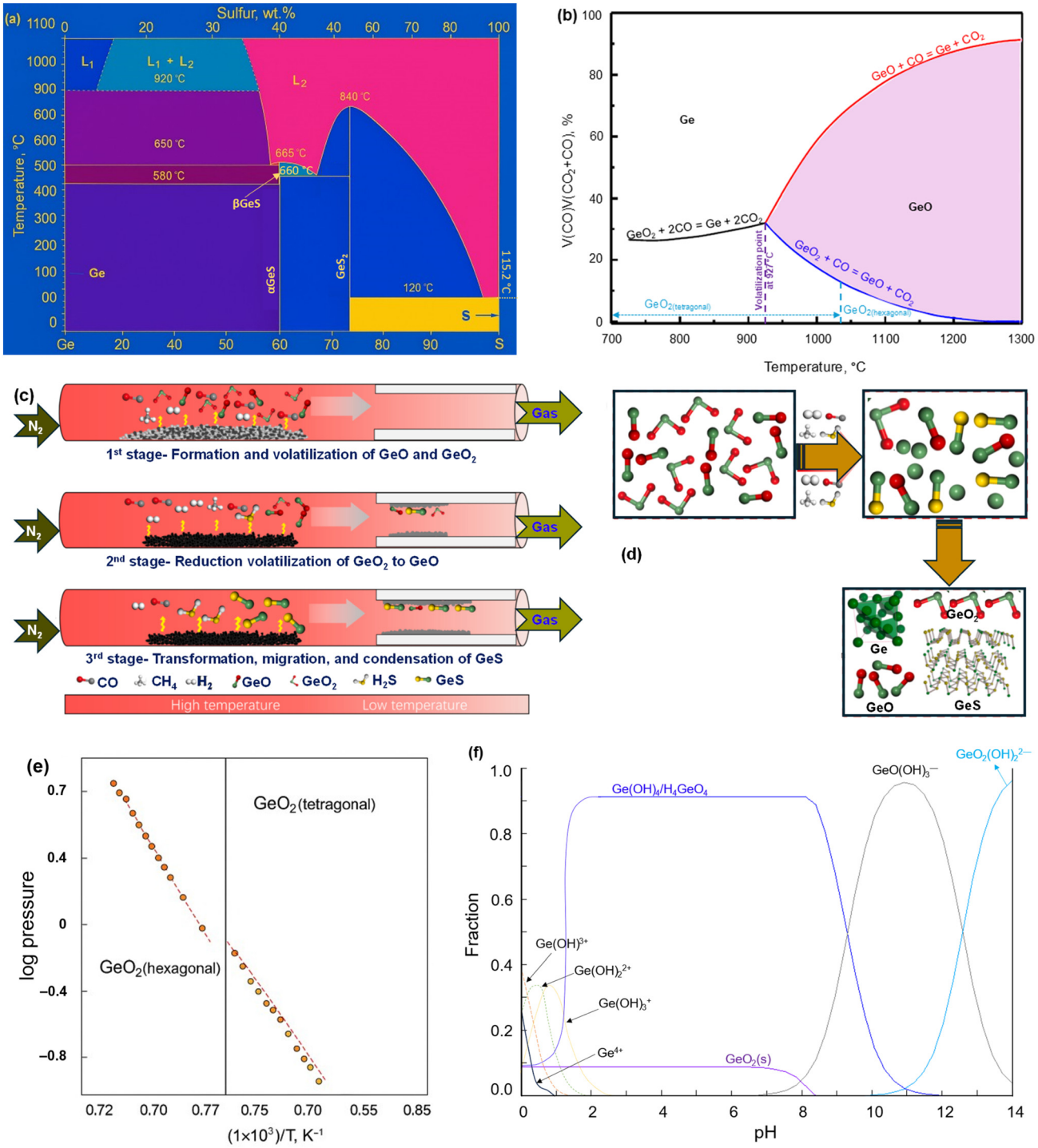

Fig. 2 Phase diagrams of germanium in the presence of [a] sulfur and [b] CO at different temperatures. [c] Mechanism of germanium migration and evolution during pyrolysis of Ge-containing lignite coal samples from Inner Mongolia coal deposits (with 197 ppm Ge). [d] Diagrams showing the transformation and condensation enrichment mechanism of different germanium species (adapted from ref. 53 with permission from Elsevier, *Sep. Purif. Technol.*, 2025, **354**, 128915, Copyright 2025). [e] Pressure *versus* temperature diagram, showing the stability of hexagonal and tetragonal GeO_2 (reproduced from ref. 57 published under open license with J-STAGE, *Journal of the Mass Spectrometry Society of Japan*, 1981, **29**(3), 249–255). [f] Distribution fraction of Ge species in aqueous solution as a function of pH, while total Ge concentration = 10 mmol at standard temperature (25 °C) and pressure (1 atmosphere).

interactions, such as those in humic acid complexes. A density functional theory (DFT) study has disclosed a large adsorption energy value of up to −8511.43 kJ mol^{-1}.[47] This indicates extremely stable associations that resist volatilization under mild thermal conditions and thus promotes germanium enrichment in combustion by-products like fly ash.[48,49]

Consequently, the concentration of Ge and its extraction efficiency greatly depend on the combustion temperature and atmosphere.[50] As can be seen from Fig. 2b, under conditions of sufficient oxygen and at a lower temperature (*i.e.*, <927 °C), a non-volatile compound GeO_2 forms in the cinder.[26] As the environment becomes more reductive, indicated by the increasing CO% in the system, metallic germanium tends to form, which is also non-volatile. However, at temperatures higher than 927 °C under a strongly reductive atmosphere, volatile GeO are generated *via* gasification that subsequently collecting enriched germanium as GeO_2 in the fly ash, as the system cools down. In contrast, coal fly ash generated *via* an integrated gasification combined cycle (IGCC) process contains a mixture of GeS_2, GeO, and GeO_2 due to exposure to liberated sulfur species.[51,52] Fig. 2c illustrates a three-step mechanism for germanium migration and evolution during lignite pyrolysis under a nitrogen atmosphere.[53] Notably, the energy input during coal burning plays a vital role in germanium recovery, with only ~60% retained in the fly ash.[54]

2.3. Phase stability and polymorphism of GeO_2

From the above discussion, it is evident that the oxidized compound, GeO_2, is the principal intermediate for metallurgical extraction of germanium. GeO_2 exhibits polymorphism with three major forms: tetragonal, hexagonal, and amorphous.[55] Each of them exhibits distinct solution chemistry properties that remain not fully understood.[40,41] Specifically, $GeO_{2(amorphous)}$ forms at ambient pressure as a network of $GeO_{4(tetrahedra)}$. On the other hand, $GeO_{2(tetragonal)}$ has a rutile structure (space group, $P4_2/mnm$) that is stable between 0 and 1035 °C, while $GeO_{2(hexagonal)}$ has an α-quartz structure (space group, $P3_221$) that is stable from 1035 to 1115 °C, with stability also influenced by partial pressure (Fig. 2c).[56,57] The GeO_2 and GeO released from the pyrolysis of lignite is reduced to GeO, GeS, and Ge^0, under the action of a reducing atmosphere such as CO, CH_4, H_2, and H_2S (Fig. 2d). Furthermore, the transition from the hexagonal to the thermodynamically stable tetragonal phase is kinetically hindered by a significant energy barrier, resulting in incomplete transformation under normal conditions. In this context, the enthalpies of GeO_2 vaporization determined by second- and third-law calculations greatly differ with the change in polymorphism between hexagonal and tetragonal (Fig. 2e). This phase transition can be facilitated by catalytic annealing and the application of high pressure.[57]

2.4. Solubility and dissolution thermodynamics of GeO_2

Haghighi and Irannajad[15] reported that $GeO_{2(tetragonal)}$ is a water-insoluble compound, which is partially true. The solubility of $GeO_{2(tetragonal)}$ varies in the range of 0.7 mg L^{-1} to 1.6 g L^{-1} with respect to temperature changes between 25 °C and 350 °C.[58] In this context, different dissociation constant values (*i.e.*, pK_a-$GeO_{2(tetragonal)}$ = 4.37 and 5.34)[59,60] have been reported, which significantly varies with pK_a-$GeO_{2(hexagonal)}$ = 1.32,[61] 1.37,[59] and 1.42.[62] Additionally, the solubility of $GeO_{2(hexagonal)}$ and $GeO_{2(amorphous)}$ has been reported as 4.53 g L^{-1} at 25 °C and 5.18 g L^{-1} at 30 °C, respectively.[55] The equilibrium of GeO_2 in water can be expressed by eqn (1),[63] with solubility increasing as the temperature (T, in Kelvin) rises, as governed by eqn (2) and (3):[64]

$$GeO_2 + H_2O \leftrightarrow Ge(OH)_4 \quad \log K = -5.02 \pm 0.13 \tag{1}$$

$$\log K_{(\text{hexagonal } GeO_2)} = 0.8114 - \frac{644.6}{T} \tag{2}$$

$$\log K_{(\text{tetragonal } GeO_2)} = 1.5276 - \frac{1975.2}{T} \tag{3}$$

Furthermore, the dissociation of $Ge(OH)_4$ into anionic species can be given as follows:

$$Ge(OH)_4 \leftrightarrow GeO(OH)_3^- + H^+ \quad pK_{a_1} = 9.32 \tag{4}$$

$$GeO(OH)_3^- \leftrightarrow GeO_2(OH)_2^{2-} + H^+ \quad pK_{a_2} = 12.5 \tag{5}$$

Conversely, the cationic species of germanium are expected to occur in highly acidic solutions of concentration above 4 mol L^{-1}.[65] The accuracy of stability values for these cationic species is debatable;[19,64] however, Marchon *et al.*[66] proposed a speciation diagram by considering Ge^{4+} with reference to the values reported by Nazarenko,[67] as shown in Fig. 2f. Subsequently, studies using advanced analytical instruments have rejected the presence of charged hydroxide species above a pH value of 0.3,[58,68] and therefore, within the pH range of 1.0 to 8.0, the major species is $Ge(OH)_4$, which transitions to anionic species of $GeO(OH)_3^-$ (or, $H_3GeO_4^-$) and $GeO_2(OH)_2^{2-}$ (or, $H_2GeO_4^{2-}$) within the alkaline pH range. Thus, the formation of Ge species as a function of pH can be summarized as follows:

$$Ge^{4+}, Ge(OH)^{3+}, Ge(OH)_2^{2+}, Ge(OH)_3^+ \overset{pH\leq 1.5}{\longleftrightarrow} Ge(OH)_4 \overset{pH=1.5 \text{ to } 9.3}{\longleftrightarrow} GeO(OH)_3^- \overset{pH=9.3 \text{ to } 12.5}{\longleftrightarrow} GeO_2(OH)_2^{2-} \tag{6}$$

The transition between these species governs the selection of extractants and precipitation agents, or determines the ion-exchange conditions during metallurgical processing. Furthermore, under specific media, germanium forms unique coordination complexes, such as H_2GeF_6 in concentrated HF (≥40%),[69] $GeCl_4$ in concentrated HCl (≥8.0 mol L^{-1}),[70] and $Ge(OH)_2(Ox)_2^{2-}$ in oxalic acid (pH 1.0–6.0).[58] Understanding the thermodynamic conditions under which these complexes are formed is essential for selective leaching and solvent extraction strategies, especially under green chemistry frameworks where organic acids or halide-free systems are preferred.

3. Germanium recovery from different sources

3.1. Aqueous-based processing of Ge-bearing materials

3.1.1. Leaching of zinc refinery residues (ZRR). As a major source of germanium (0.04–0.5 wt%), zinc refinery residues

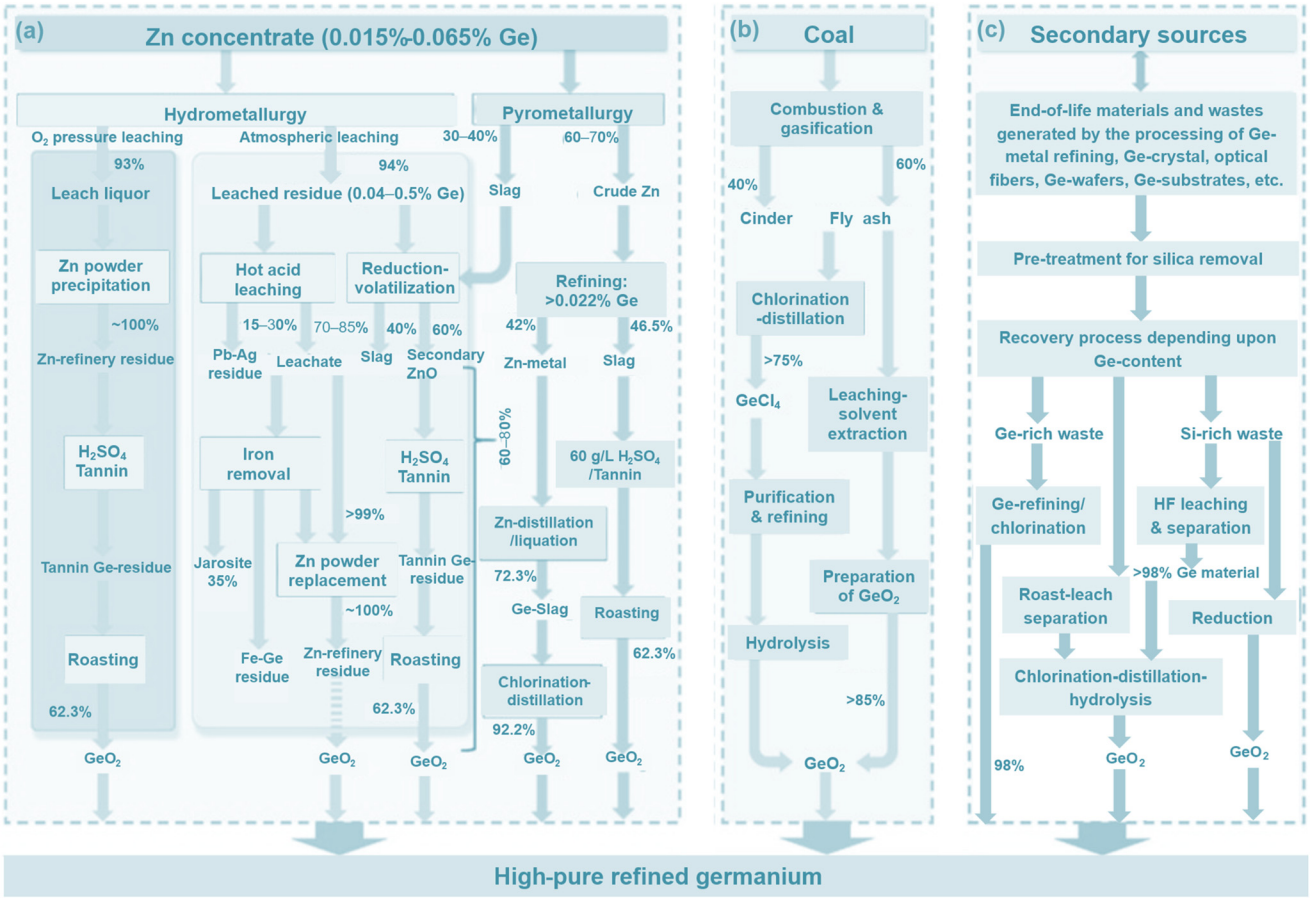

Fig. 3 Illustration of different processing flow diagrams for germanium extraction from industrial residues of [a] zinc plant mainly through sphalerite ore and [b] coal-burnt fly ash, and [c] *via* recycling by urban mining end-of-life materials (modified from ref. 26 with permission from Elsevier, *J. Clean. Prod.*, 2021, **294**, 126217, Copyright 2021).

(obtained through different routes of zinc extraction processes as shown in Fig. 3a) have been processed to recover germanium as a by-product of zinc processing by dissolving them in hot H_2SO_4 solution along with zinc, copper, and iron. At a lower temperature of 60 °C, Ge^{4+} can be selectively leached over copper although the maximum efficacy was found to be less than 80%.[71] Although zinc and iron were separated easily using cementation, precipitation, and solvent extraction techniques, the co-dissolution of SiO_2 in H_2SO_4 solution to form colloidal silica and silica gel is observed to be a major issue that inhibits the leaching yield by affecting solid–liquid interactions. The filtration rate of the leached slurry is slowed and germanium entrapped within the silica gel is lost.[72] The leaching reaction under acidic conditions can be written as follows:

$$GeO_2 + SiO_2 + 2H_2SO_4 \rightarrow Ge(SO_4)_2 + SiO_2 \cdot H_2O_{(polymerized)} \quad (7)$$

When the ZRR contains 10% SiO_2, only 57% of the germanium is leached with hot H_2SO_4.[73] To overcome this issue, it has been reported that HF leaching dissolves silica to freely mobilize germanium into the solution.[74,75] Silica-gel formation can be controlled by pressure leaching. Jiang *et al.*[76] reported a 10% improvement in leaching yield of germanium (efficiency 99.7%) in comparison with that of ambient leaching (efficiency 89.5%) when secondary ZnO was subjected to a pressure oxidative leaching process. These reports clearly showed that germanium dispersed in different minerals like wurtzite and galena could be liberated through breaking the mineral sulfide structure by pressure oxidation, which is not possible during ambient leaching without introducing a highly oxidative environment. However, loss of Ge cannot be due to its hydrolytic precipitation along with iron and co-adsorption onto the precipitate surface.[31] In alternative approaches, additives like $Ca(NO_3)_2$, H_2O_2, NaClO, and MnO_2 have been introduced into the Ge-recovery system,[77,78] revealing the effectiveness of nitrate in enhancing germanium leaching while calcium in sulfate solutions forms columnar gypsum that led to smooth filtration.[77] The leaching of germanium *via* chlorination with HCl has also been explored where silica is controlled in the leached solution, which subsequently undergoes distillation and captures $GeCl_4$ of low boiling point (*i.e.*, 83.1 °C),[78] although simultaneous hydrolysis of $GeCl_4$ takes

place to revert germanium to its GeO_2 form at low acid concentration and low temperature. The reactions can be understood as follows.[79]

In the presence of concentrated HCl:

$$GeO_2 + 4HCl \rightarrow GeCl_4 + 2H_2O \quad (8)$$

In the presence of diluted HCl at 0 °C:

$$GeCl_4 + 2H_2O \rightarrow GeO_2 + 4HCl \quad (9)$$

The HCl concentration is generally greater than 7.8 mol L^{-1} (preferably concentrated HCl is used), below which chlorination may not be completed, whereas a $H_2O:GeCl_4$ ratio of 1 : 3 has been suggested to inhibit the formation of $Ge(OH)_4$.[79] The purified GeO_2 that is obtained *via* eqn (9) is then subjected to hydrogen reduction at 650 °C for 5–8 h to metallize germanium through eqn (10) and (11), during which Ge can be melted by raising the temperature to 1000 °C to recover O_2-free Ge metal; however, the process requires re-melting, casting and zone-refining to yield highly pure semiconductor grade germanium (*i.e.*, element of 6 N purity):[80]

$$GeO_2 + H_2 \rightarrow GeO + H_2O \quad (10)$$

$$GeO + H_2 \rightarrow Ge^0 + H_2O \quad (11)$$

Due to the disadvantages of low efficiency, prolonged processing, and high cost associated with the equipment for converting $GeO_2 \rightarrow Ge^0$, direct H_2 reduction of $GeCl_4$ has been explored by following eqn (12), although this is also a very complex system. Vorotyntsev *et al.*[81] and Kadomtseva *et al.*[82] have shown that the adsorption of H_2 molecules by $GeCl_4$ vapor is followed by the formation of Ge^0 with a lower activation energy (35 kJ mol^{-1}) in the presence of a W-based catalyst when compared with the uncatalyzed reaction (48 kJ mol^{-1}).[83] On the other hand, Kornev *et al.*[84] showed that the temperature greatly influences the reduction process when using a plasma-chemical reduction method. As can be seen from Fig. 4a, at a $H_2/GeCl_4$ ratio of 15, the condensed Ge is formed within the range of 1250–1500 K, while the compounds $GeHCl_3$, GeH_2Cl_2, and GeH_3Cl form within the range of 300–1580 K, 500–1580 K, and 760–1500 K, respectively:

$$GeCl_4 + H_2 \rightarrow Ge^0 + 4HCl \quad (12)$$

Besides the use of mineral acids, organic acid has also been employed for Ge leaching, yielding 98.8% germanium in the leach liquor by using 110 g L^{-1} $H_2C_2O_4$ at 40 °C,[85] and ~93% germanium using 100 g L^{-1} tartaric acid at a higher temperature of 80 °C.[86] Improved leaching efficiency is achieved with oxalic acid and can be expressed as:[87]

$$GeO_2 + 2HC_2O_4^- \rightarrow [Ge(OH)_2(C_2O_4)_2]^{2-} \quad (13)$$

The addition of H_2O_2 (0.12 mol L^{-1}) has also been suggested for efficiently dissolving insoluble Ge species like Ge^0, GeS_2, and GeS that somehow could not be oxidized properly during the roasting process of ZnS ore. The improved

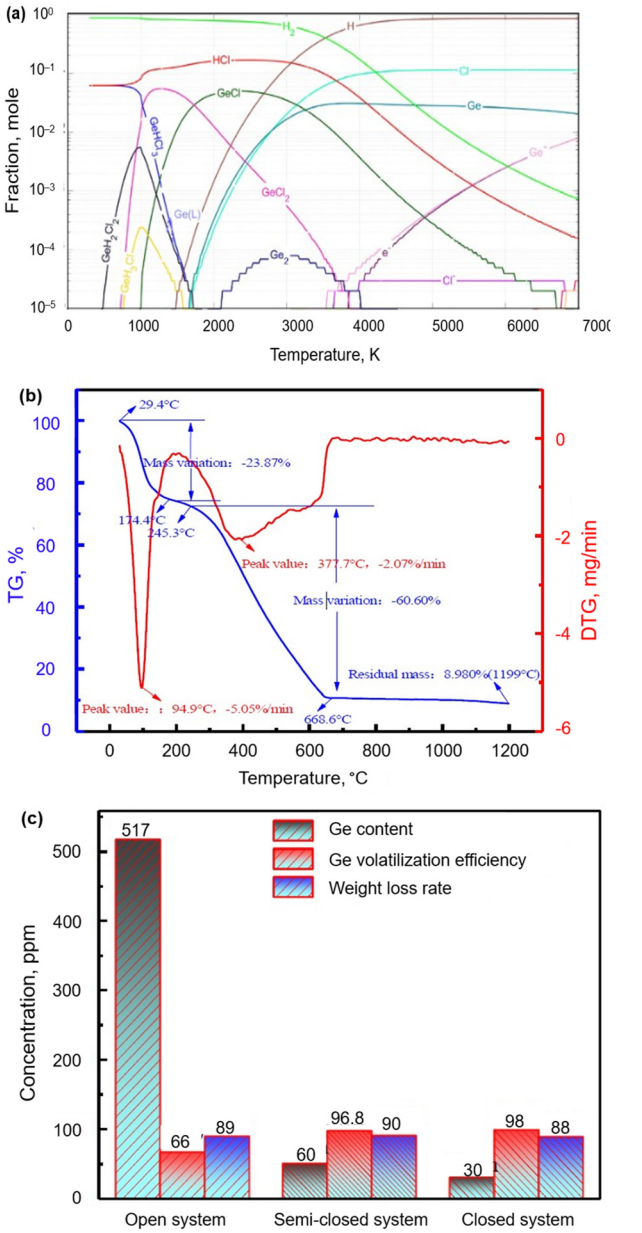

Fig. 4 [a] Equilibrium mole fractions of reaction products as a function of temperature for the ratio of $GeCl_4/H_2$ = 15, with a plasma pressure of 760 Torr (adapted from ref. 84 published under open use license with MDPI, *Sci.*, 2024, **6**(1), 1). [b] Thermogravimetric analysis curve for the reduction of Ge-bearing lignite coal, and [c] effect of roasting on Ge volatilization under the operating conditions of temperature, 1100 °C; air flow rate, 0.7 L min^{-1}; heating rate, 8 °C min^{-1}; and holding time, 180 min (adapted from ref. 99 published under open use license with MDPI, *Materials*, 2023, **16**(15), 5374).

leaching yield of Ge can be highlighted through the following exothermic reactions:[88]

$$GeS_2 + 8H_2O_2 \rightarrow GeO_2 + 2SO_4^{2-} + 4H^+ + 6H_2O \quad (14)$$

$$Ge + 2H_2O_2 \rightarrow GeO_2 + 2H_2O \quad (15)$$

$$GeS + 4H_2O_2 \rightarrow GeO + SO_4^{2-} + 2H^+ + 3H_2O \quad (16)$$

Iron leached into the oxalate solution can be quantitatively assessed by introducing an ultrasound-assisted iron powder replacement, which also reduces the loss of germanium by co-precipitation through optimizing the Fe[total]/Fe(III) mole ratio value at 6. In comparison with the oxalate precipitation wherein germanium losses occur due to co-precipitation/occlusion,[88] the beneficial application of the ultrasound-assisted technique can be ascribed to the negative pressure created by ultrasonic cavitation in the liquid. This subsequently disrupts the liquid by producing many bubbles and generates shear forces that break the occluded particles to liberate the entrapped Ge. The reaction occurs as follows:

$$2Fe(C_2O_4)^+ + Fe + C_2O_4^{2-} + 2H_2O \xrightarrow{\text{ultrasound}} 3FeC_2O_4 \cdot H_2O \quad (17)$$

The use of ultrasonic-assisted pickling has also been suggested for the removal of zinc, iron, magnesium, and arsenic impurities from the Ge–tannin residue under conditions of 0.2 mol L^{-1} H_2SO_4, pulp density 30%, pickling time 30 min, and temperature 40 °C.[89] It was observed that an increase in acid concentration tends to result in loss of Ge, whereas the pickling behavior attributed to cavitation effects can destroy the packaging of particles and increase the contact area of solid–liquid interactions. In general, the use of ultrasonic-assisted leaching showed an improved leaching yield for Ge of about 3–5% compared with regular leaching (without ultrasonication).[90]

The formation of a refractory ferrite ($ZnFe_2O_4$) mineral phase has been commonly observed in zinc roasting, which hinders the leaching yield of germanium entrapped therein. To deal with these types of residues, two-step sulfuric acid leaching can be applied, first to leach out 92% zinc and second to leach out 94% copper, which yields a 300% enrichment of germanium in the residue.[88] The subsequent leaching of the Ge-bearing residue in 70 g L^{-1} oxalic acid at 90 °C yielded 99% germanium in the leach liquor. In another study by Rao *et al.*,[91] the acid-treated residue was leached in 1.0 mol L^{-1} NaOH at a pulp density of 5%, temperature of 80 °C, and time of 4 h, yielding ~90% germanium although 33% lead and ~70% silicon were present in the leach liquor as well. Alkali leaching of germanium can be expressed as follows:

$$GeO_2 + 2NaOH \rightarrow Na_2GeO_3 + H_2O \quad (18)$$

An inability to control the co-dissolution of metals at a higher concentration clearly indicates the superiority of H_2SO_4–$H_2C_2O_4$ leaching systems, wherein <2% of silicon dissolution occurs.[45]

3.1.2. Leaching of coal-based resources (CBR; coal, cinder, and fly ash). Although coal in the working beds is characterized by its extremely low germanium content (usually 1–3 g t^{-1}),[92] coal-based resources are important sources of germanium as 20–30% of the global production of this critical metal is contributed to by coal cinder and fly ash processing.[21] Although direct distillation and inorganic acid leaching of coal powder can be applied to Ge extraction, traditionally this route has been identified as being uneconomical for industrial application.[93] However, in the recent past, the growing importance of germanium has prompted researchers to explore this route with renewed interest. Wei and Rimmer[94] demonstrated that sequential leaching of high-quality Ge-bearing coal using HCl and HF solutions can achieve up to 100% cumulative dissolution efficiency of Ge. Their analysis revealed that germanium in coal samples is either weakly bound to organic matter, probably through chelation, or it remains associated with fine-grained minerals closely linked to the organic matrix, thereby enabling it solubilization in HCl–HF media. An industrial alternative involves chlorination distillation of Ge-bearing soot derived from coal combustion and gasification, wherein HCl leaching facilitates the formation of $GeCl_4$ (refer to Fig. 3b). The resulting $GeCl_4$, with a low boiling point (83.1 °C), can be further processed,[78] as discussed in Section 3.1.1.

The rapid depletion of high-germanium-content coal is a matter of concern, whereas low-grade coal remains unexploited owing to economic reasons;[95,96] hence, coal combustion is a good way to enrich germanium *via* fly ash.[97,98] Yang *et al.*[99] studied reductive volatilization of Ge-bearing lignite that yielded 71 600 ppm germanium in fly ash as compared to an initial content of only 30 ppm. As per the results of thermogravimetric analysis shown in Fig. 4b, the weight loss of 26.23% up to 174.4 °C is accounted for by the evaporation of inherent moisture in the lignite. A sharp reduction in weight from 245.3 °C is attributed to the combustion of lignite carbon, while heating to above 668.6 °C results in the weight loss becoming more moderate at only 6.55% (accounting for only 7.20% of the total weight loss) due to the decomposition of carbonate and sulfate. At temperatures above 927 °C, the reduction process for GeO_2 in coal (refer to Fig. 2b) can be written as follows:

$$GeO_2 + C \rightarrow GeO + CO \quad (19)$$

The reduction system significantly influences Ge volatilization and its subsequent enrichment (see Fig. 4c). When Ge-bearing coal is combusted in an open-door muffle furnace, the germanium concentration in the residual mass reached ~517 ppm, while it was only 60 ppm and 30 ppm when the combustion was performed in a semi-closed and fully closed furnace, respectively. This disparity can be explained by the influence of oxygen availability on the redox environment. In an open system, the presence of oxygen suppresses the reductive conditions required for GeO_2 conversion to volatile GeO (as shown in Fig. 2b), thereby favoring the formation of non-volatile GeO_2 in the residual ash. As a result, germanium remains concentrated in the solid phase rather than volatilizing into the gas phase.

Because hexagonal GeO_2 in fly ash is water-soluble,[32,51] leaching experiments using deionized water and wastewater collected from different sections (*i.e.*, gas cooling system,

cooling chamber, and desulphurization scrubbing) of an integrated gasification combined cycle (IGCC) plant have been conducted. The highest leaching efficiency (84%) was achieved using deionized water at room temperature (25 °C).[52] When increasing the temperature to 150 °C, the leaching efficiency could not be improved any further, which somehow departs from expectations based on thermodynamic eqn (2). However, when leaching was performed in the presence of air/O_2,[100] both the rate and selectivity of Ge extraction improved, with concentrations rising from 25 ppm to over 50 ppm across a temperature range of 25 °C to 90 °C over a 6 h period. Similarly, the water leaching of Puertollano IGCC fly ash at 90 °C yielded up to 80% Ge dissolution.[48,101] This behavior can be attributed to the precipitation of iron oxyhydroxides at a greater rate in the presence of air/O_2 and the oxidation of sulfur species to soluble sulfates, which facilitate germanium release from the IGCC fly ash.

Arroyo *et al.*[101] used different lixiviants (other than water) such as H_2SO_4, HCl, CaO, and NaOH with the oxidant H_2O_2, and a variety of complexing agents (including oxalic acid, $H_2C_2O_4$ and catechol, $C_6H_6O_2$) for a comparative leaching study of germanium from Puertollano IGCC fly ash. The leaching order obtained was $H_2C_2O_4$ > $C_6H_6O_2$ > H_2SO_4 HCl > H_2O > HCl > H_2O_2 > NaOH > CaO. The results demonstrated that efficient and rapid leaching can be achieved with oxalic acid (83% Ge in 2 h), which can be attributed to germanium forming anionic species (as shown in eqn (13)) while iron is precipitated as insoluble oxalate. On the other hand, the inhibited leaching with CaO can be ascribed to a greater concentration of dissolved salts hindering Ge dissolution from the fly ash particles.[52,100]

3.1.3. Leaching of e-waste materials. About 30% of available germanium is used in semi-conductors and optical fibers.[102] Hence, electronic items discarded as end-of-life e-waste have been identified as valuable and concentrated secondary sources of germanium. For instance, the non-magnetic fraction of diodes may contain up to 0.5% germanium,[103] while optical fibers can hold as much as 4% in the form of GeO_2.[104] Gupta and Mudhar[70] proposed an extraction process involving leaching semiconductor waste with 2.0 mol L^{-1} HCl, yielding germanium quantitatively as $GeCl_4$ in the leached solution. Furthermore, using a more concentrated HCl solution (6.0 mol L^{-1}) has been shown to extract over 98% germanium from Zener diodes at 80 °C within 3 h.[105]

The use of H_2SO_4 resulted in poor leaching yields of below 10%,[106] possibly due to germanium adsorption onto *in situ* precipitated silica,[107] which comprises ~96% of the weight fraction in optical fibers. This yield was greatly improved by adding 5 vol% HF into 0.1 mol L^{-1} H_2SO_4 solution, over a period of 3 h while leaching was performed at room temperature (25 °C) only, demonstrating how the behavior of silica influences Ge recycling.[106] However, to avoid the use of HF in leaching processes, NaOH roasting was performed at 500 °C with a high NaOH-to-SiO_2 mole ratio (up to 6). The roasted mass was subsequently leached with H_2SO_4 solutions, yielding >99% dissolution efficiency.[108,109] This favorable leaching outcome is attributed to the formation of the anionic species $H_2GeO_4^{2-}$ at pH values above 12.5 (refer to Fig. 2c). Lee *et al.*[110] later replaced NaOH with Na_2CO_3, conducting roasting at 700 °C for just 1 h. This approach enabled complete germanium recovery (26 ppm) from optical fiber waste *via* HCl leaching, revealing the strong affinity of Na_2CO_3 for silica to form sodium silicate shown as follows in eqn (20):

$$SiO_2 + Na_2CO_3 \rightarrow Na_2SiO_3 + CO_2 \quad (20)$$

However, the recycling of waste solar panels studied by Kuroiwa *et al.*[111] showed that both HF and NaOH are required to destroy the silicate structure to liberate germanium from the panel surface. In an alternative approach, Rafiee *et al.*[103] employed acetic acid for germanium leaching, achieving over 70% extraction from diode samples using 2.5 mol L^{-1} CH_3COOH solution at 90 °C for 4 h. They disclosed that the organic acid leaching follows three different phases: (i) a diffusion-controlled stage during the initial 5 min, (ii) interfacial mass transfer during the intermediate stage, and (iii) product-layer control near the completion of the leaching process. For the diffusion-controlled region, the rate coefficients were determined to be 6.61×10^{-5}, 6.94×10^{-5}, and -6.87×10^{-5} at CH_3COOH concentrations of 2.5 mol L^{-1}, 5.0 mol L^{-1}, and 7.5 mol L^{-1}, respectively. The leaching reactions in acetic acid follow eqn (21)–(23):

$$CH_3COOH \leftrightarrow H^+ + CH_3COO^- \quad (21)$$

$$GeO_2 + 4CH_3COO^- + 4H^+ \rightarrow Ge(CH_3COO)_4 + 2H_2O \quad (22)$$

$$GeO_2 + 4H^+ \rightarrow Ge^{4+} + 2H_2O \quad (23)$$

Based on the literature survey, the leaching processes applied to the extraction of germanium from different primary and secondary resources are presented in Table S1. It summarizes the optimized conditions, Ge yield, and salient features of the studied hydrometallurgical processes.[112–114]

Germanium recovery *via* recycling waste photovoltaic panels (conducted following plastic removal) has been examined alongside the generation of hydrogen and magnesium phosphate fertilizer as by-products.[115] Initially during this process, Ge-bearing PV scrap was treated with Mg scrap at 400 °C, while maintaining a heating rate of 15 °C min^{-1}, to form Mg germanide and/or silicide.[116] The reaction endpoint was monitored *via* pressure changes, and after the system returned to its initial pressure value, the heating was stopped and the sample retrieved from the furnace. The resulting magnesium germanide and/or magnesium silicide (see eqn (24)), was then hydrolyzed with 25 wt% H_3PO_4 at ambient temperature to leach germanium (see eqn (25)):

$$2Mg_{(s)} + Ge/Si_{(s)} \rightarrow Mg_2Ge/Si_{(s)} \quad (24)$$

$$Mg_2Ge/Si_{(s)} + H_3PO_4 \rightarrow Mg(HPO_4)_{(aq)} + (Ge/Si)_nH_{(2n+2)} \quad (25)$$

Subsequently using a low-vacuum phosphate reduction process, hydrogen gas and magnesium phosphate fertilizer were generated as valuable by-products.[117] Thermodynamic

analysis of the process indicated the decomposition of the phosphate reductant into products such as $Na_4P_2O_7$, $Na_5P_3O_{10}$, PH_3, O_2, and H_2. Depending on the temperature zones within the reactor, three distinct morphological and elemental phases involving Ge, P, and O were observed, aligning with the reaction order models for phosphate-mediated reduction. Stage I, occurring in the temperature range of 500–673 K, mainly involved the decomposition of NaH_2PO_2. The decomposition products were mainly P(v)-containing compounds $Na_4P_2O_7$ and $Na_5P_3O_{10}$, and also PH_3, H_2, and H_2O. Stage II begins when the temperature is increased to around 953 K, which is marked by further weight loss attributed to the reduction of GeO_2 by the strong reducing gases of PH_3 and H_2. The different reactions are represented by eqn (26)–(29) leading to the condensation of germanium species including elemental Ge (Ge^0), divalent Ge (Ge^{2+}), and a minor fraction of tetravalent Ge (Ge^{4+}). The decomposition of sodium hypophosphite (NaH_2PO_2) proceeded *via* hydrolysis followed by a nucleophilic addition–elimination mechanism. This reaction pathway generates PH_3 and H_2, which act as reductants and facilitate the breakdown of the GeO_2 octahedral structure, leading to the formation of elemental Ge^0 and its oxides (as illustrated in Fig. 5). Under optimized conditions, specifically at 1173 K and a reaction time of 40 min, the process achieved a germanium volatilization efficiency exceeding 90%:

$$4GeO_2 + 2PH_3 \rightarrow 4Ge^0 + P_2O_5 + 3H_2O \quad (26)$$

$$8GeO_2 + 2PH_3 \rightarrow 8GeO + P_2O_5 + 3H_2O \quad (27)$$

$$GeO_2 + 2H_2 \rightarrow Ge^0 + 2H_2O \quad (28)$$

$$GeO_2 + 2H_2 \rightarrow GeO + H_2O \quad (29)$$

In another study focused on germanium recovery from optical fiber waste,[118] carbothermal reduction of GeO_2 revealed a dynamic transformation in the reaction pathway. Although the transition zone between intermediates was not sharply defined, it was observed that GeO was initially formed and desorbed from the reaction zone. This intermediate was then further reduced to elemental germanium (Ge^0), which became the dominant product. However, the evaporation of Ge^0 occurred at a significantly slower rate compared to GeO. Spectroscopic analysis confirmed the coexistence of metallic impurities, including Zn, Cu, and Mg, within the product matrix. These impurities are believed to interfere in product purity and disrupt the morphology of the recovered material.

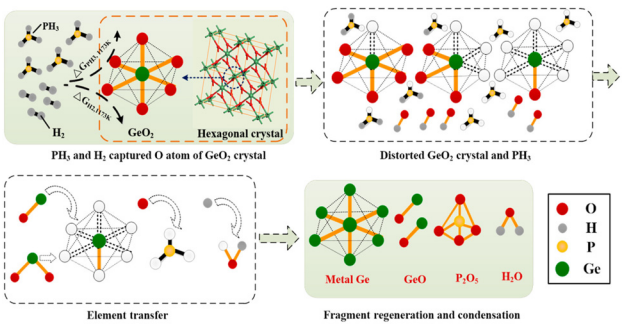

Fig. 5 Reaction mechanism of the vacuum phosphate reduction of GeO_2 (adapted from ref. 117 with permission from the American Chemical Society, *ACS Sustain. Chem. Eng.*, 2019, 7(2), 2176–2186, Copyright 2018).

Several methods have been disclosed for germanium recycling from e-waste materials *via* pre-heat treatment followed by hydrometallurgical leaching. The roasted mass predominantly containing germanium and/or its oxides undergoes chlorination leaching to form $GeCl_4$.[119,120] In a unique method, the digestion of waste solar film in sodium hypochlorite followed by NaOH leaching at 90 °C for 30 min has been disclosed.[121] By adding a certain amount of precipitant and water, the pH was adjusted to values in the range of 4.5–6.5 using HCl under slow stirring, to precipitate a Ge-enriched mass, which subsequently undergoes distillation with HCl to collect the $GeCl_4$ product. The stepwise reactions take place as follows:

$$Ge + 2NaClO + 2NaOH \rightarrow Na_2GeO_3 + 2NaCl + H_2O \quad (30)$$

$$Na_2GeO_3 + 2HCl \rightarrow GeO_2 \downarrow + 2NaCl + H_2O \quad (31)$$

$$GeO_2 + 4HCl \rightarrow GeCl_4 + 2H_2O \quad (32)$$

3.2. Germanium separation from leach liquors

3.2.1. Tannin precipitation. Precipitation remains one of the most widely adopted industrial techniques for metal recovery from aqueous solutions. In the context of Ge recovery from ZRR leachates, tannin-based precipitation has been practiced for decades. In this process, organic tannins act as precipitants, forming insoluble tannin–germanium complexes by binding with germanium oxide anions in solution.[122] The precipitated complex is subsequently oxidized using reagents such as $NaClO_3$ or $KMnO_4$, and then, the intermediate is dissolved in hydrochloric acid to produce $GeCl_4$. Pure germanium tetrachloride is finally obtained through calcination.[123] In industrial applications, tannins like tannic acid ($C_{76}H_{52}O_{46}$), which contains hydrolyzable polyphenols with multiple *ortho*-phenolic hydroxyl groups, are commonly used.[124] The precipitation mechanism is primarily governed by coordination between germanium ions and the phenolic hydroxyl groups of tannin molecules.[30] According to orbital hybridization theory, tannins ionize in acidic media to form phenoxy anions, which then coordinate with germanium through Ge–O covalent bonds involving sp^3d^2 hybridization, resulting in a stable six-coordinate complex (see Fig. 6a).[125,126]

However, tannic acid's chelating behavior is not selective to germanium alone; it also complexes with Fe^{3+} and precipitates other impurities such as Cu^{2+}, Zn^{2+}, and Pb^{2+}, thereby compromising the purity of the Ge precipitate.[30] For example, increasing the dosage of tannic acid from 0.1 g to 0.2 g can raise the Ge precipitation yield from 10% to 91%, but simultaneously increases iron co-precipitation from negligible levels to 52%.[127] This highlights the trade-off between higher yields

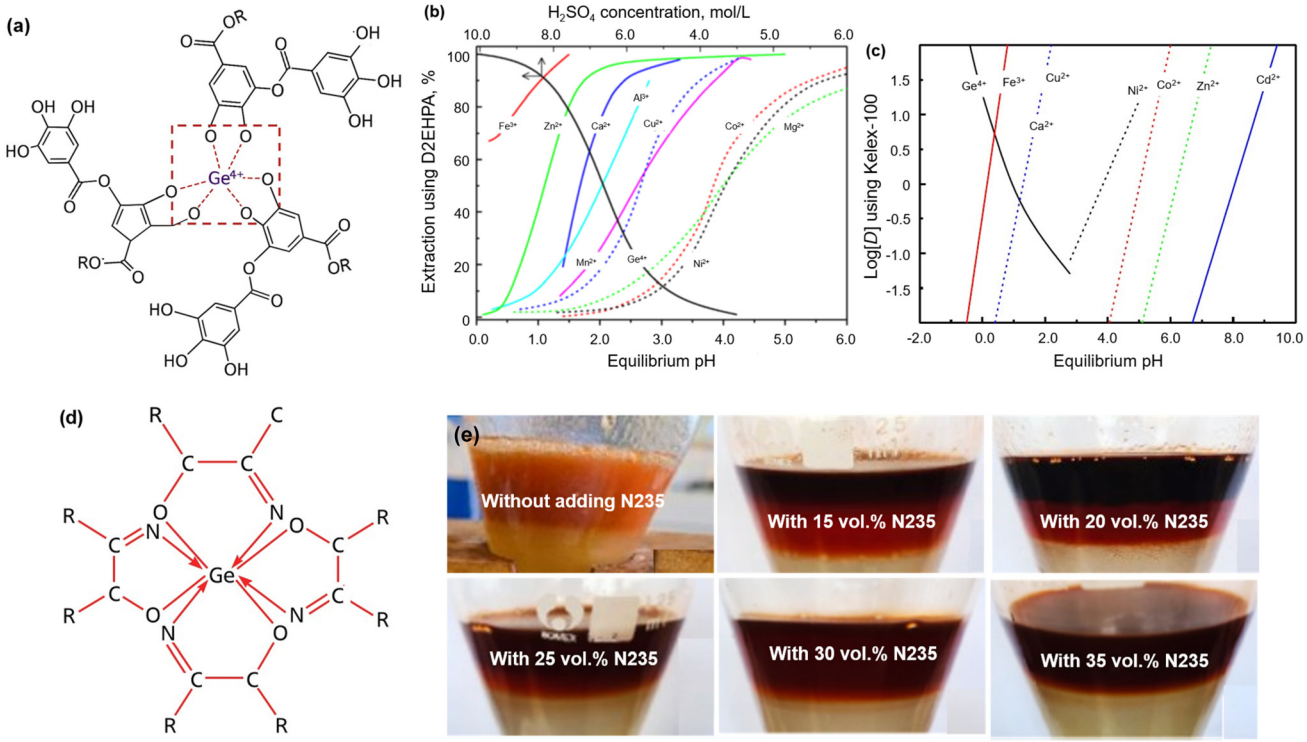

Fig. 6 [a] A representation of tannin-germanium chelation formed during precipitation from acidic solutions (adapted from ref. 126 published under open use licence with MDPI, *Metals*, 2023, **13**(4), 774.); [b] pH-isotherm of possible metals in Ge-bearing sulfate solutions as a function of equilibrium pH and H_2SO_4 concentration; and [c] logarithmic distribution of germanium between organic and aqueous phases as a function of equilibrium pH (reprinted and modified from ref. 26 with permission from Elsevier, *J. Clean. Prod.*, 2021, **294**, 126217, Copyright 2021). [d] Ge-chelation complexation into the extract phase using oxime-based chelating extractant. [e] Phase disengagement effect in Ge-extraction as a function of N235 concentration, while maintaining the organic-to-aqueous phase ratio = 1 : 2, H_2SO_4 concentration into aqueous feed = 67.13 g L^{-1}, D2EHPA concentration into the organic phase = 30%, contact time = 5 min, and temperature = 25 °C (adapted from ref. 143 with permission from Elsevier, *Sep. Purif. Technol.*, 2024, **329**, 125175, Copyright 2024).

and lower selectivity at elevated tannin dosages. Furthermore, excess tannic acid leads to emulsification during the precipitation and purification steps. These emulsified residues can burn on electrode surfaces during subsequent zinc electrolysis, increasing energy consumption and lowering current efficiency.[128] To enhance selectivity, multi-stage precipitation processes are often employed, but they increase operational complexity, cost, and volume requirements.[123]

To address volume and selectivity challenges, Li *et al.*[129] proposed a two-stage counter-current precipitation approach for sulfate leach solutions containing zinc. However, they noted that lower tannic acid dosages significantly reduced Ge recovery. In their study, achieving 99.5% Ge precipitation at pH 2.5 and 50 °C while operating a 20-minute contact time required a tannic acid dosage 25 times higher than the stoichiometric amount. In a few studies, such as that of Drzazga *et al.*,[130] higher precipitation temperatures (up to 90 °C) have been investigated, but these pose another issue: tannic acid begins to degrade above 70 °C, making such conditions unsuitable.[131] Due to limitations, such as poor selectivity, high reagent consumption, emulsification issues, and thermal instability, the use of tannin-based precipitation for germanium recovery has been largely phased out and replaced by more advanced liquid–liquid and solid-phase extraction techniques (discussed in subsequent sections).

3.2.2. Liquid phase (solvent) extraction. Solvent extraction (SX) is a widely applied liquid–liquid separation technique conducted by employing mainly four types of organic extractants, *i.e.*, phosphoric acid derivatives as proton exchangers, oxime-based chelating extractants, amine-based anion exchangers, and neutral extractants.[132] Based on the functional group associated with carbon chains, their extraction ability differs with respect to the acid concentration in the feed solution or the equilibrium pH. They exhibit good quantitative extraction efficiency for germanium under certain conditions; however, co-extraction of iron is a major issue. Because phosphoric acid derivatives (*e.g.*, di-2-ethyl-hexyl-phosphoric acid, D2EHPA or P204 and bis(2,4,4-trimethylpentyl)dithiophosphinic acid, Cyanex 301) can absorb ferric iron at very low pH values (see Fig. 6b), their applicability is somehow disadvantageous, which can be overcome by applying oxime-based extractants (*e.g.*, 5,8-diethyl-7-hydroxydodecane-6-oxime, LIX 63, alkyl-substituted 8-hydroxyquinoline, LIX 26, and hydroxamic acid, HGS98). As can be seen from Fig. 6c, under highly acidic conditions, oxime-based extractants selectively exclude trivalent iron to promote chelation of Ge^{4+} species into the organic

phase. This favorably formed tetravalent species of Ge^{4+} by metal chelation is depicted in Fig. 6d. The extraction equilibrium for the extractants D2EHPA and LIX (commonly represented as $\overline{(RH)_2}$) can be written as follows:

$$Ge^{4+} + 4\overline{(RH)_2} \leftrightarrow \overline{(Ge)_2(R_2H)_4} + 4H^+ \quad (33)$$

In sulfuric acid media, the extraction of Ge^{4+} using D2EHPA can be maximized at acid concentrations >8.0 mol L^{-1}. Under such highly acidic conditions, co-extraction of other metals is difficult, as illustrated by the extraction isotherms of metals with D2EHPA in Fig. 6b. However, the presence of highly concentrated free acid in the raffinate poses disadvantages. Hence, to address this, 7-(4-ethyl-1-methyloctyl)-8-hydroxyquinoline—known as Kelex 100 (denoted by $\overline{HL}$)—is preferred for recovering Ge species from strongly acidic H_2SO_4 solutions (pH < 0). The extraction reaction proceeds as follows:[65]

$$Ge(OH)_i^{(4-i)} + 3\overline{(HL)} + HSO_4^- + (i-3)H^+ \leftrightarrow \overline{GeL_3HSO_4} + iH_2O \quad (34)$$

A study conducted by Ma *et al.*,[133] demonstrated that a mixture containing 30% P204 and 15% of an ester, namely tributyl phosphate (TBP, $(RO)_3$–P═H), achieved an extraction efficiency of >94% for Ge^{4+}. It has been suggested that TBP assists by enhancing the extraction by stabilizing the cationic Ge^{4+} species through partial anionic charge thereby reducing both the anion potential and the degree of ion hydration.[134] About 19% of iron was co-extracted into the organic phase, which was subsequently scrubbed using 6 mol L^{-1} HCl. Germanium was quantitatively stripped from the organic phase using 250 g L^{-1} NaOH solution at an organic-to-aqueous (O/A) phase ratio of 2.

Notably, Harbuck *et al.*[74] reported that of the many organic extractants, only Kelex 100, LIX 26, LIX 63, and Cyanex 301 can exhibit effective germanium extraction from sulfuric acid media, with relative performances ranked as Kelex 100 ~ LIX 26 < LIX 63 < Cyanex 301.[65,70,135,136] Germanium can be successfully recovered from solutions containing large amounts of acid (at pH ≤ 0) *via* ion-pair formation into the organic phase, whereas under low acidity (pH ≥ 1.0) conditions, extraction efficiency is poor due to the prevalence of neutral complexation.[65] The extraction rate using Kelex 100 can be improved by adding *n*-octanol, and quantitative extraction is achievable by operating under a mixed regime of both diffusion and the chemical reaction.[135] In contrast, the first commercially available α-hydroxyoxime (*i.e.*, LIX 63) for Ge extraction from sulfate media requires high concentrations (no less than 1.0 mol L^{-1}) of LIX 63 in the organic phase and contact with aqueous solutions containing >1.0 mol L^{-1} H_2SO_4.[137,138] Synergistic extraction strategies have been developed that involve adding different organophosphorus acids, *e.g.*, octylphenyl acid phosphate (OPAP),[138] 2-ethylhexyl phosphonic acid mono 2-ethylhexyl ester (Ionquest 801),[139] highly branched C_{10} tertiary carboxylic acid (Versatic acid 10),[140] D2EHPA,[141] and another oxime, LIX 26, into LIX 63, which could significantly dilute the need for α-hydroxyoxime molecules in the organic phase.[142] The synergistic extraction mechanism using the LIX 63 + Ionquest 801 system is written as:[26]

$$Ge(SO_4)_2 + \frac{1}{2}\overline{RH} + \frac{1}{2}\overline{HA} + \frac{1}{2}H_2SO_4 \leftrightarrow \overline{Ge(SO_4)_2(RH)_{0.5}(HA)_{0.5} \cdot (H_2SO_4)_{0.5}} \quad (35)$$

A new synergism, comprising C_{7-9} hydroxamic acid (YW100) with D2EHPA has been reported by Tan *et al.*[143] The extraction of cationic Ge^{4+} from sulfuric acid solution could be improved *via* reducing the hydrolysis loss of YW100 and improving phase separation performance when the trioctyl tertiary amine (N235) is introduced into the organic phase at different concentrations. It has been observed that in the absence of N235, the hydrophilic groups of YW100 led to a reduction in its solubility in the organic phase, thereby forming an emulsion with greater extraction of germanium and the appearance of a third phase (Fig. 6e). The resultant enhanced extraction efficiency resulted in reduced recovery of germanium *via* loss of metal in this third phase. As the N235 was introduced into the organic phase, extraction efficiency decreased to 81% at 35 vol% N235, but the organic phase could be quantitatively stripped using NH_4F solution, which improved the overall recovery of germanium during the extraction process. An optimized organic mixture of 3 vol% YW100 + 15 vol% D2EHPA + 35 vol% N235 + 47 vol% kerosene achieved 99.4% extraction efficiency. Subsequent stripping using 1.0 mol L^{-1} NH_4F solution enabled recovery of 96.2% Ge from the extract phase.

Using Kelex 100 and LIX 63 alone revealed extraction efficiency in the order of $Cl^- < NO_3^- < I^- \ll CNS^-$ but slower kinetics was exhibited with thiocyanate media, which can be improved by adding Cyanex 301 to synergize the process.[144] Additionally, the mixing of 2 vol% hydroxamic acid (HGS98) with 5 vol% D2EHPA could result in an extraction efficiency of 99%,[145] although the hydroxamic acid has the disadvantage of lower chemical stability with higher water solubility.[144,146] Additionally, iron when forming anionic species at higher acidic concentrations, particularly in HCl media, renders it difficult to apply amine-based extractants (*e.g.*, N235). Besides the predominant formation of $GeCl_4$, the extraction of anionic species such as $[Ge(OH)_nCl_{(6-n)}]^{2-}$ has been reported by Sargar and Anuse[147] when using N-*n*-octylaniline. The stepwise protonation of an amine extractant $\overline{(RR'NH)}$ followed by an extraction reaction can be expressed as follows:

$$\overline{RR'NH} + HCl \leftrightarrow \overline{RR'NH_2^+Cl^-} \quad (36)$$

$$2\left[\overline{RR'NH_2^+Cl^-}\right] + [Ge(OH)_nCl_{(6-n)}]^{2-} \leftrightarrow \left[\overline{(RR'NH_2^+)_2[Ge(OH)_nCl_{(6-n)}]^{2-}}\right] + 2Cl^- \quad (37)$$

Meanwhile, amine extractants have found improved applicability for recovery of anionic species of germanium in organic acids. The complexation mechanism for tertiary amine salts (represented by $\overline{R_3NH^+X^-}$) extracting anionic Ge oxalate[34] and

quaternary ammonium salts (written as $\overline{R_4N^+X^-}$) extracting Ge tartrate[148] can be given as follows:

$$2\left[\overline{R_3NH^+X^-}\right] + \left[Ge(OH)_2(C_2O_4)_2\right]^{2-} \leftrightarrow \left[\overline{(R_3NH^+)_2[Ge(OH)_2(C_2O_4)_2]^{2-}}\right] + 2X^- \quad (38)$$

$$\left[\overline{R_4N^+X^-}\right] + \left[Ge(OH)_2(HT)\right]^- \leftrightarrow \left[\overline{R_4N^+[Ge(OH)_2(HT)]^-}\right] + X^- \quad (39)$$

The extraction efficiency and selectivity of Ge–tartaric acid complexes over co-existing metals ions (such as zinc, cadmium, copper, and nickel) reach a maximum when the molar ratio of $C_4H_6O_6$ to germanium is increased. This is due to the higher stability constant of Ge–tartaric acid complexes relative to those formed with other metals at pH ~1.0.[149,150] In contrast, the use of alternative complexing agents such as oleic acid and catechol results in markedly lower germanium extraction efficiencies, decreasing from ~100% to below 5% and ~85%, respectively. In the case of the tertiary amine (N235), 93.5% germanium and about 7% arsenic were extracted from a tartrate solution of pH 1.2.[36] The co-extraction of arsenic could be controlled by adding TOPO as a phase modifier with N235, yielding extraction efficiencies for germanium with different ligands that followed the order tartaric acid (95.8%) > citric acid (71.7%) > gallic acid (46.6%) > oxalic acid (<5%) > salicylic acid (less than 5%).[151] Replacing TOPO with TBP as a modifier further improved extraction efficiency and phase separation compared to using the amine solvent alone.[106] Drzazga *et al.*[152] successfully achieved > 99% germanium extraction from sulfate solutions at pH values in the range of 1–3 using a TOA–TBP system, following prior complexation with tartaric acid, leaving indium in the raffinate, which was subsequently extracted using D2EHPA. For stripping germanium from the organic phase, NaOH solutions in the range of 10–20% were found effective. Below 10% NaOH, germanium is precipitated, while concentrations above 20% NaOH led to third-phase formation and emulsion instability.

Using a phosphonium-based salt, namely trihexyl(tetradecyl)phosphonium bis-2,4,4-(trimethylpentyl)phosphinate (Cyphos IL104, denoted as $\overline{R_3R'\ P^+A^-}$), the extraction equilibria determined at 3.0 mol L^{-1} and 6.0 mol L^{-1} HCl have been commonly given according to eqn (40).[105] The change in aqueous media could drastically reduce the extraction efficiency to below 5% with HNO_3 and H_2SO_4 solutions (in the concentration range of 1–10 mol L^{-1}). This again shows the inability of Ge forming stable anionic species in these media:

$$\left[\overline{R_3R'\ P^+A^-}\right] + Ge^{4+} + 6Cl^- + 2H^+ \leftrightarrow \left[\overline{(R_3R'\ P^+)_2GeCl_6{}^{2-}}\right] + 2[HA] \quad (40)$$

Under comparable conditions, the extraction efficiency exhibited the order of quaternary ammonium salts > tertiary amine > dithiophosphinic acid; however, the high consumption of complexing agents and low selectivity of Ge extraction over some heavy metals (*e.g.*, arsenic) have also been observed.[36] On the one hand, either using a higher concentration of HCl in ZPR leaching or in the presence in solution of higher chloride content, $GeCl_4$ species are formed, which can be extracted by using neutral extractants (*e.g.*, TBP and 4-trialkylphosphine oxides, *e.g.* Cyanex 923; commonly represented as $\bar{L}$) *via* adduct formation following the solvation mechanism as follows:

$$GeCl_4 + 2\bar{L} + xH_2O \leftrightarrow \overline{GeCl_4 \cdot 2L \cdot xH_2O} \quad (41)$$

$$Ge(OH)_4 + 2\bar{L} + xH_2O \leftrightarrow \overline{Ge(OH)_4 \cdot 2L \cdot xH_2O} \quad (42)$$

Using 20 vol% Cyanex 923 in the organic phase, an extraction efficiency for Ge of about 100% could be achieved from an oxalate solution (0.15 mol L^{-1} $C_2H_2O_4$) within an extraction pH range of 1.0–3.0.[149] The extraction equilibrium forming the Ge–oxalate complex with the phosphine oxides is given in eqn (43). As is evident from Fig. 6(b–d), Ge extraction takes place under acidic conditions, hence, its quantitative stripping from the loaded organic phase is carried out in alkaline solution to recover germanium into the aqueous solution, forming the anionic $[H_3GeO_4]^-$ and $[H_2GeO_4]^{2-}$ species:[76]

$$H_2Ge(C_2O_4)_3 + 4\bar{L} \leftrightarrow \overline{H_2Ge(C_2O_4)_3 \cdot 4L} \quad (43)$$

Based on the literature reviewed, the separation and recovery techniques applied to Ge recovery from various leach liquors generated by the processing of different primary and secondary resources of this critical metal have been presented in Table S2. This table summarizes the optimized conditions, yield and selectively, and salient features of the reported liquid and solid phase separation techniques.[153–157]

3.2.3. Solid phase extraction. Analogous to the liquid–liquid extraction process, the ion-exchange (IX) technique uses liquid-to-solid mass transport from aqueous solution to resin beads containing the exchangeable functional group/ions. The same fundamentals are used as with SX; therefore, the chelating and anion exchange resins are largely employed either to complex germanium *via* ion exchange or to be adsorbed onto the resin surface by subsequent chelation of Ge^{4+} (under highly acidic pH conditions) and exchange of oxoanions (under basic pH > 9.0 conditions), respectively. The low concentration of germanium in leach liquor supports its applicability for efficient and economic recovery but at a much slower rate of mass transfer than that for SX.

Various commercially available resins can be employed, such as Amberlite IRA-743, WP-2, and Lewatit TP-260,[158] methylglucamine-based resins,[159] and those resins functionalized with diol groups and saccharides,[160] including catechol and catechol-8-hydroxyquinoline resins.[161] Among these, bifunctional *N*-methylglucamine resins exhibit quantitative adsorption of $GeO(OH)_3^-$ and $GeO_2(OH)^{2-}$ species (by dissociating $Ge(OH)_4$ at pK_a > 9.0) *via* coordination between glucose sites and nitrogen-containing groups. In multi-metal systems, Ge adsorption was decreased by competing ions, with iron exerting a particularly detrimental influence on the adsorption

process.[158] The sorption capacity of 1,2-diol-type resins was found to be lower than that of *N*-methylglucamine resins, *i.e.*, 0.96 mmol g^{-1}, but exhibited reduced selectivity for germanium.[19,159] However, capacities improved to 1.5–2.4 mmol g^{-1} at pH 7.0–7.8, which approaches similar sorption capacity values of mannose-functionalized chitosan resins (*i.e.*, 2.4 mmol g^{-1})[160] and di(2-hydroxyethyl)amine-type cellulose derivatives (*i.e.*, 1.8 mmol g^{-1} at pH 8.0), which is almost three times greater than sorption capacity values for 2-hydroxyethylamine-type cellulose derivatives.[162] At pH values above 4.0, catechol forms a stable, negatively charged complex with germanium as shown in eqn (44).[163] This complex exhibits a highly symmetric three-dimensional structure more stable than the corresponding silicate ionic complex,[164,165] as illustrated in Fig. 7a.

$$Ge(OH)_4 + 3C_6H_4(OH)_2 \leftrightarrow Ge(C_6H_4O_2)_3^{2-} + 2H^+ + 4H_2O \quad (44)$$

Cruz *et al.*[161] studied the effect of different proportions of catechol by mixing Ge species with 8-hydroxyquinoline resin and observed that catechol alone yielded the best separation performance for germanium over silicon (Fig. 7b). The addition of 8-hydroxyquinoline into the resin mass facilitates the separation over Zn (Fig. 7c) but not copper in the mixed solution (Fig. 7d), whereas the equilibrium involving quaternary ammonium resins (*e.g.*, Amberlite IRA-900 and IRA-958) employed for Ge adsorption from the catechol complex can be given as follows by eqn (45):[33]

$$\overline{2R_2NR_3Cl} + Ge(C_6H_4O_2)_3^{2-} \leftrightarrow \overline{(R_2NR_3)_2Ge(C_6H_4O_2)_3} + 2Cl^- \quad (45)$$

Additionally, Amberlite IRA-900 and IRA-958 exhibited good selectivity for Ge adsorption (96% and 89%, respectively) over that for other metal ions,[164] justifying their theoretical affinity with anionic resins in the order of Ge > V > Sb > Mo > As > Ga > Zn, Co, Ni, Mn.[33] Very recently, selective anion exchange for germanium separation was reported using D201 × 7 resin after converting $Ge(OH)_4$ into anionic species $[GeO_2(OH)_2C_4H_4O_4]^{2-}$ by adding tartaric acid (at a 1 : 1 molar ratio with respect to the Ge concentration) into sulfuric acid-leached solution.[166] The observed sorption followed the Langmuir isothermal model and exhibited pseudo-second-order kinetics with a maximum uptake capacity of 214 mg g^{-1} and enrichment factor of 74.7. The metal complexation and schematic of the IX -mechanism are illustrated in Fig. 7e. An anion-exchange membrane (RX-1, polystyrene trimethylammonium) has also been applied to adsorb the anionic Ge–catechol complex from aqueous media containing silicon as the major impurity.[111,163] Experimental results showed active ionic interactions at pH 11.0 as the solution was allowed to permeate through the RX-1 membrane.[165]

Among limited studies, Patel and Karamalidis[167] used microwave-based synthesis to functionalize polystyrene beads with catechol, nitro-catechol, and pyrogallol that yielded maximum sorption capacities of 29.76 mg g^{-1}, 39.14 mg g^{-1}, and 37.13 mg g^{-1}, respectively. The synthesized sorbents were highly selective for germanium, showing no adsorption for the competitive metal ions at pH 1–2. Activated carbon has been applied to Ge adsorption when maximum sorption capacity

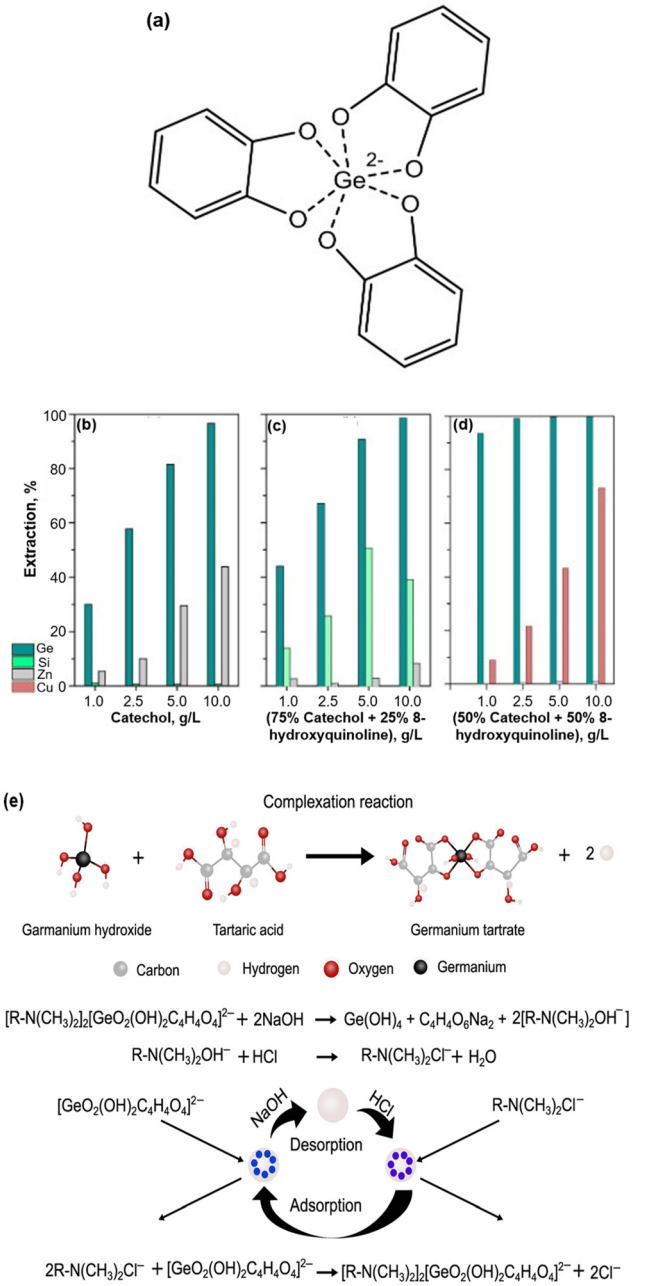

Fig. 7 [a] Structure of the anionic Ge–catechol complex. The ion-exchange extraction behaviour of metal ions with different resins made of [b] 100% catechol, [c] 75% catechol + 25% hydroxyquinoline, and [d] 50% catechol + 50% hydroxyquinoline, while varying the resin-to-liquor ratios in the range of 1–10 g L^{-1} (modified and reproduced from ref. 161 with permission from Elsevier, *Sep. Purif. Technol.*, 2018, **193**, 214–219, Copyright 2018). [e] A previous formation of anionic Ge–tartrate species that undergoes ion-exchange adsorption with chloride-functionalized D201 × 7 resin, followed by Ge desorption into NaOH solution (modified and reproduced from ref. 166 with permission from Elsevier *Hydrometallurgy*, 2024, **224**, 106230, Copyright 2024).

values of 5.6 mg g^{-1} and 10.5 mg g^{-1} at pH 5.0 were exhibited while using H_3PO_4-treated carbon powder (point of zero charge, pzc at 3.8) and untreated carbon powder (pzc value, 7.1), respectively.[168,169] Due to the pzc values, the negative surface charge in pH > 7.1 media decreased the adsorption, whereas the positive surface charge at lower pH (~1.0) exhibited negligible adsorption for the cationic species of germanium (refer to Fig. 2c). Xiang *et al.*[170] synthesized three chitosan-based adsorbents by grafting *p*-hydroxybenzoic acid (HBA-CS), 3,4-dihydroxybenzoic acid (DBA-CS), and 3,4,5-trihydroxybenzoic acid (TBA-CS) to study steric effects on Ge adsorption caused by the differing amounts of phenolic hydroxyl. The results were correlated with the arrangement of the active adsorption sites following the order of TBA-CS > DBA-CS > HBA-CS > CS. The steric effect of TBA-CS was found to be more ideal than that of DBA-CS due to more phenolic hydroxyl groups, which exhibited superior affinity towards Ge $(OH)_4$.

4. Germanium flow, life-cycle, and economic analyses of extraction processes

4.1. Germanium flow and life-cycle assessment

The static flow and stock data of germanium have been summarized by Wong *et al.*[171] in order to comprehensively track its flow throughout the life cycle. Using these data, a material flow chart has been plotted as shown in Fig. 8a, revealing that about 113 t of germanium is sourced from coal ash, and 53 t from ZRR. The refined Ge output totalled about 87 t, while 79 t are lost as tailings and slag, resulting in a recovery rate of only 52%. Secondary supply *via* urban mining contributed 19 t of recycled Ge as new scrap. During the refining and manufacturing stages, Ge-bearing materials are processed into various products. Of the 111 t of refined germanium allocated to different applications, China consumed 56 t alone, while exports were directed primarily to the EU (43%) and the US (47%). At the end-of-life stage, waste stocks mainly consist of scrap from the fiber and IR optics sectors. However, germanium embedded in PET and satellite components is completely unrecoverable.[172]

Subsequently, life-cycle assessment (LCA), a crucial decision-making tool for evaluating environmental impacts,[173–176] has been employed to analyze various Ge-recovery routes within this framework. The primary extraction of germanium is mainly performed through the energy-intensive smelting of zinc and lead ores; however, the environmental burdens of germanium extraction have traditionally been attributed to its mother metals, fostering the perception that germanium extraction itself has relatively low environmental impacts.[173] Therefore, an accurate assessment of the environmental impacts of germanium extraction from the starting raw materials is imperative, yet it remains a relatively underexplored topic in Ge metallurgy. Notably, fewer than 2% of published studies have provided comprehensive inventory data necessary for robust LCA modeling.[177,178]

Recent studies have attempted to address this knowledge gap by conducting cradle-to-gate LCAs on various germanium recovery routes. Within the LCA framework, the output of a functional unit of 1 kilogram of germanium crystals was established to analyze three major processes under the defined boundary conditions as represented by the dotted lines in Fig. 3.[178] Within the standard framework of ISO:14040 and ISO:14044, openLCA was used for evaluating the environmental indicators (refer to Table S3 for the indicators with respective units in the SI), while following the methodology defined in the International Life Cycle Database (ILCD, v1.0.8). Among the three different feed material systems, System 1 involved ZRR with Pb concentrate as the feed raw material to a smelter for up-concentration of germanium, followed by chlorination to $GeCl_4$, hydrolysis to GeO_2, reduction to Ge metal, and zone refining to recover Ge crystals. In System 2, ZRR underwent a similar series of steps, but without mixing with Pb concentrate, thereby eliminating the need for smelting during processing, while in System 3 ZRR is sent to a smelter. Furthermore, considering a mixed feed in Systems 1, 2, and 3 at a mass ratio of 4 : 1 : 1, data obtained from electro-optic materials (Umicore, Belgium) were used to evaluate the LCA for environmental indicators.[179,180] Table S3 shows the midpoint impact category results with global warming potential (GWP) value of 852 kg CO_2-eq for 1 kg of Ge crystals in terms of the baseline scenario.

On the other hand, considering an output of 1 kg of Ge crystals from coal burning (bearing 600 ppm Ge) and recuperation of the coal fly ash that achieves a concentration of <0.3%, Robertz *et al.*[177] studied the LCA within the system boundary (as defined in Fig. 3b). They used data from region-specific electricity grid mix for Umicore (Belgium) and the National Chinese grid mix (China), while excluding downstream solid waste and wastewater treatment processes. Recognizing the uncertainties in the concomitant energy recovery from coal, they considered two different cases: (i) no energy recovery from Ge-rich coal, and (ii) energy production from coal in a power plant that was assumed to produce a suitable germanium concentrate. Consequently, they obtained the GWP values of 5566 kg CO_2-eq and 698 kg CO_2-eq, respectively. The coal burning activity produces ample amounts of heat/energy, hence, the second case with 698 kg CO_2-eq of GWP seems to be a realistic value. As shown in Fig. 8b, the main contribution to the environmental impact is linked to the coal raw material, either with the emissions during its burning or with its extraction and treatment. Coal particularly affects the impact categories of freshwater eutrophication (>99%), ecotoxicity for aquatic fresh water (60%), and freshwater consumption (50%).

When the LCA was performed for Ge recovery *via* the recycling of e-waste material within a silica matrix containing 3.5% germanium, the scraps are considered burden free, but the transport of the scraps to the production plant is included in the LCA study, following the hydrometallurgical system boundary (defined in Fig. 3c). The study showed that the main

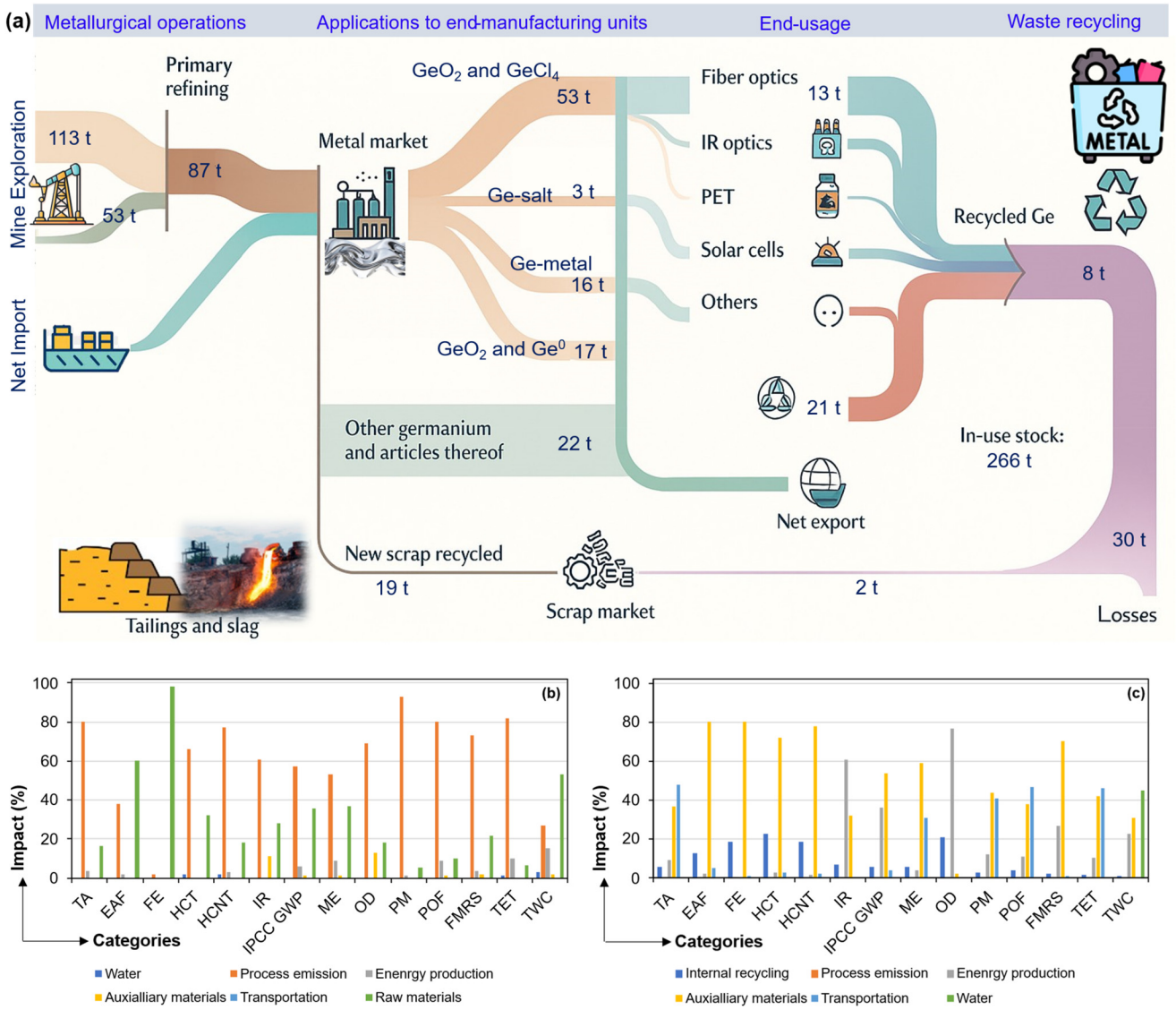

Fig. 8 [a] Diagram illustrating the static flows and stocks of germanium. The environmental impact analysis for germanium extraction from [b] coal and [c] PV production scrap *via* the hydrometallurgical route. The impact categories can be referred to as TA = terrestrial acidification (H^+ mole-eq), EAF = ecotoxicity for aquatic freshwater (CTU-eq), FE = freshwater eutrophication (kg P-eq), HCT = human carcinogenic toxicity (CTUh), HCNT = human non-carcinogenic toxicity (CTUh), IR = ionizing radiation (kg U_{235}-eq), IPCC GWP = global warming potential (kg CO_2-eq), ME = marine eutrophication (kg N-eq), OD = ozone depletion (kg CFC11-eq), PM = particulate matter (kg PM2.5-eq), POF = photochemical ozone formation (kg NMVOC), FMRS = fossil and mineral resource scarcity (kg Sb-eq), TET = terrestrial ecotoxicity (mole N-eq), TWC = total freshwater consumption (kg).

contributors to the impact categories are linked to the energy sources and the chemicals used for the leaching and chlorination process (refer to Fig. 8c).[177] The auxiliary materials have high impacts with respect to every category except ozone depletion. The transportation of raw materials also contributes significantly to the environmental burden through acidification potential, marine and terrestrial eutrophication, particulate matter, and photochemical ozone formation. Overall, the GWP for recycled germanium was found to be a substantially lower value of 163 kg CO_2-eq, which can be further reduced to 151 kg CO_2-eq if HCl could be recycled from the chlorination-refining step to the acid-leaching step.[177] However, a separate study by Hoof *et al.*[178] reported a higher GWP value of 280 kg CO_2-eq, likely due to the use of pyrometallurgical processes involving high temperatures. This discrepancy underscores the environmental advantage of hydrometallurgical recycling methods for germanium recovery. Furthermore, a sensitivity analysis focusing on the fossil and mineral resource scarcity (FMRS) indicator, of particular relevance to both the EU and US, revealed a variation of 6 to 11 orders of magnitude depending on the depletion model used. These large variations were largely driven by the germanium content of the input feedstock, indicating that higher Ge-bearing feed can substantially reduce its criticality to improve the supply chain of this valuable element.

4.2. Economic analysis of the extraction processes

The economic feasibility of germanium recovery from different sources is influenced by several interrelated factors, including the concentration of germanium in the material, the scale and availability of feedstock, the complexity of extraction technologies, and the potential for co-recovery of other valuable elements. This section critically assesses the economic viability of germanium extraction from ZRR, CBR, and e-waste, which represent the major sources of this strategically important element.

Industrial residues generated during zinc smelting are currently the most economically viable source of germanium. These materials typically contain relatively high germanium concentrations, ranging from 100 to 600 ppm. More importantly, their processing is often integrated into existing hydrometallurgical and pyrometallurgical workflows within the zinc industry, allowing for the co-recovery of germanium with minimal additional infrastructure or energy input. From an economic standpoint, the high throughput of zinc smelters and the established logistics for residue handling significantly lower the marginal cost of germanium recovery. However, reliance on ZRR inherently ties the supply of germanium to the zinc production cycle. Any downturn in zinc output can limit germanium availability. Furthermore, certain residues may require pretreatment to remove impurities or improve recovery efficiency, which can slightly increase the operational costs. Despite these limitations, the mature industrial context and consistent germanium yields make ZRR the most commercially attractive source currently in use.

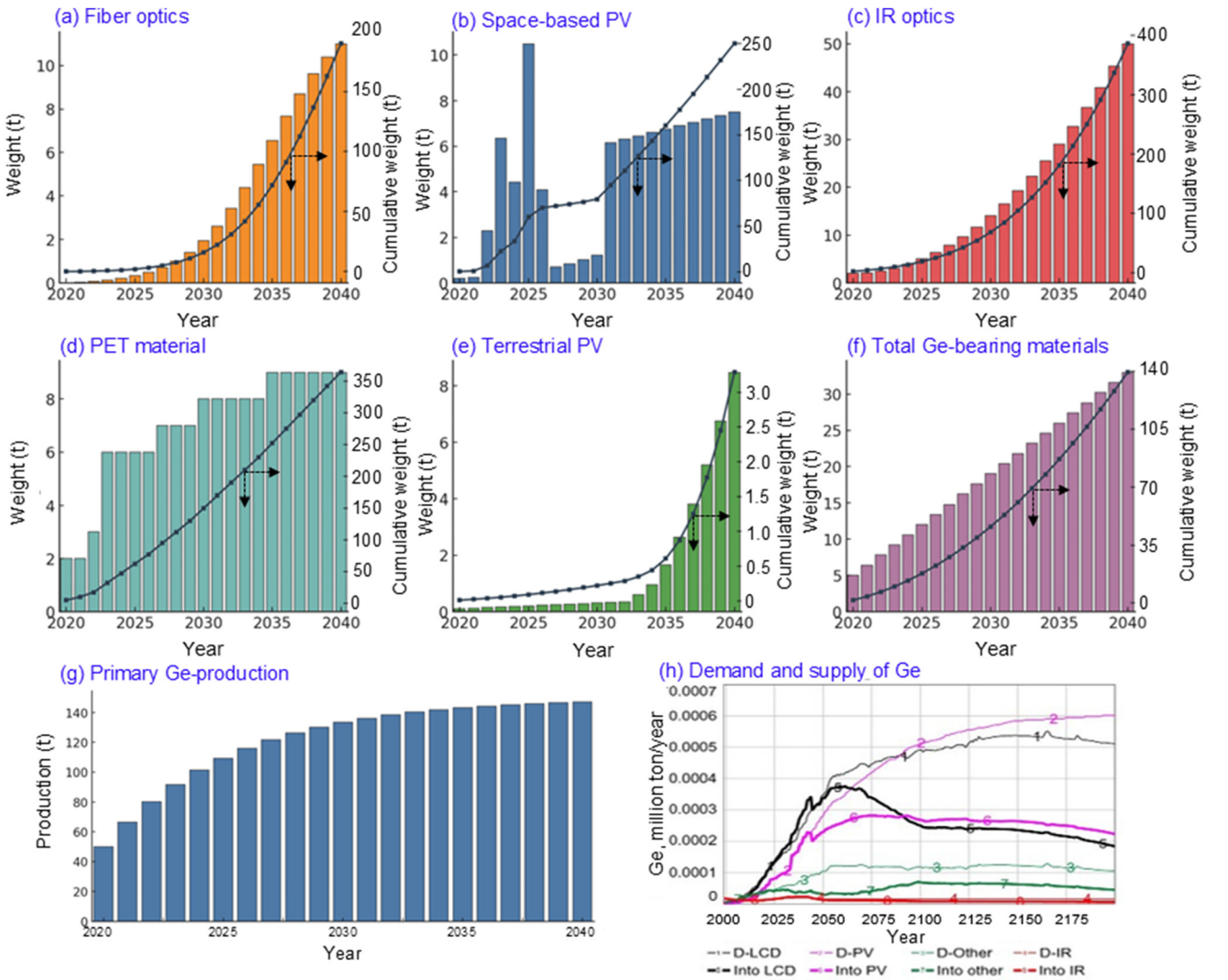

Fig. 9 Projection of primary production and scrap generation of germanium from [a] fiber optics, [b] space-based PV, [c] IR optics, [d] PET catalysts, [e] terrestrial PV, [f] total Ge-bearing scrap generation, and [g] prediction for primary Ge-production. [h] The simulated results of demand and supply for germanium into different application areas, wherein, the thin line represents sector-specified demand (abbreviated as 'D'), and the thick line shows actual supply of germanium (abbreviated as 'Into') (adapted from ref. 184 under open use license with Springer Nature, *Biophys. Econ. Sust.*, 2024, **9**, 5, Copyright 2024).

In the case of CBR, it is produced in vast quantities worldwide as a by-product of coal combustion and is readily available at minimal acquisition cost. Some deposits, particularly those originating from lignite or low-rank coal in regions such as Inner Mongolia and parts of Eastern Europe, exhibit elevated germanium concentrations (exceeding 100 ppm), making them more suitable for economic recovery. Moreover, the potential for co-extraction of rare earth elements and other

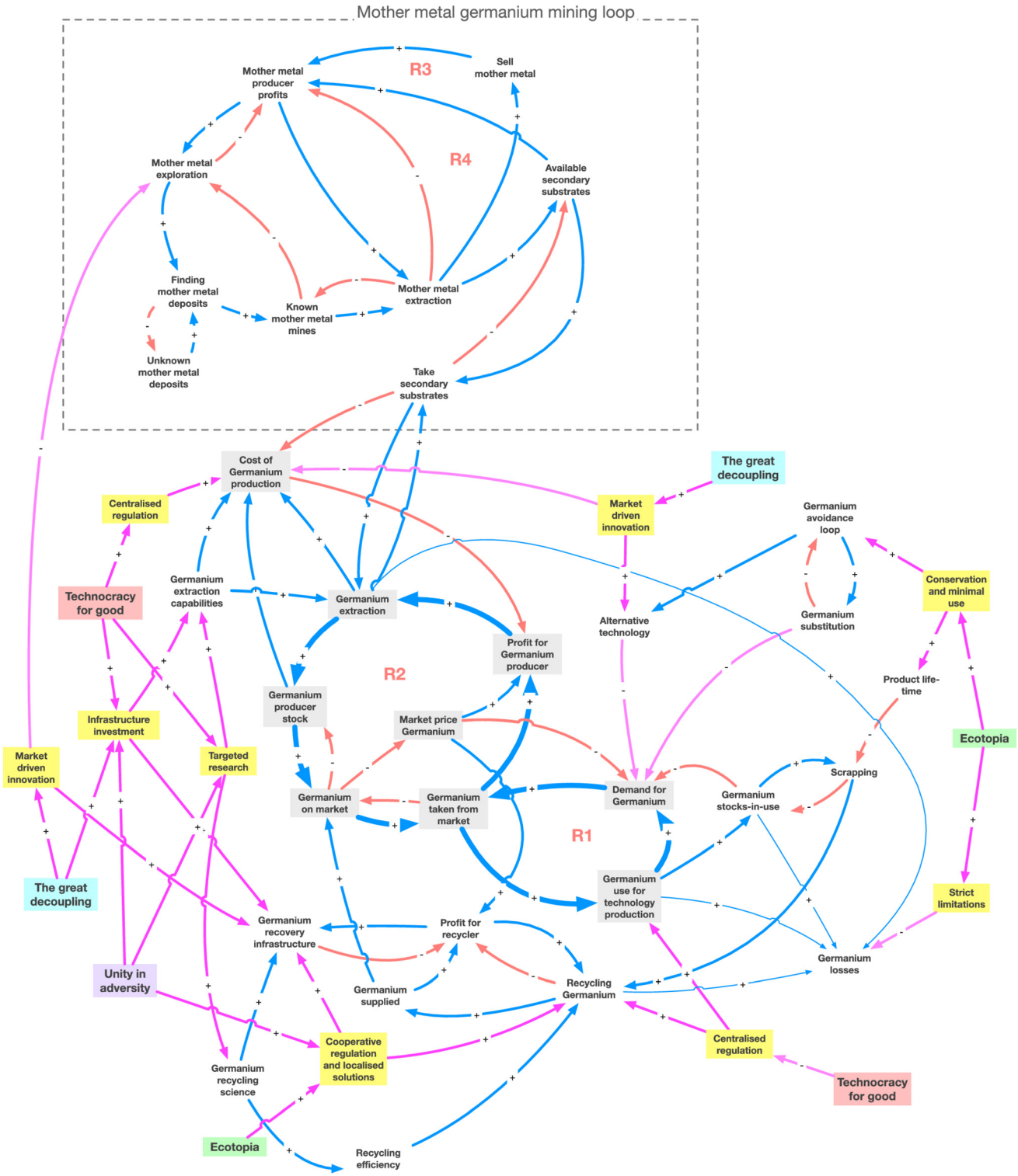

Fig. 10 The pathways towards each of the imaginaries are illustrated with different policy domains that are required to be in place for each of the imaginaries to be achieved (adapted from ref. 184 under open use license with Springer Nature, *Biophys. Econ. Sust.*, 2024, **9**, 5, Copyright 2024).

trace metals presents opportunities for process integration and cost sharing. Nevertheless, most CBR contains germanium in the range of 5 to 50 ppm, which is often too low to justify standalone recovery operations. Additionally, extraction methods tend to be chemically intensive, involving acid or alkali leaching, thermal activation, or pressure treatment, each contributing to increased operational costs. The highly variable composition of CBR and its dispersed nature further complicate economic scaling. As a result, while CBR can be economically viable in geographically specific, high-grade deposits, its general viability is limited by low germanium content and relatively high processing costs.

E-waste is emerging as a major alternative source of germanium, distinguished by its high Ge content in certain components. Specific electronic products, such as infrared optical devices, high-frequency semiconductors, and photovoltaic cells, may contain germanium concentrations ranging from 0.1 to 1 wt%, far exceeding levels found in ZRR or CBR. When recovery processes are focused on these high-value components, the economics can be favorable. Additionally, the concurrent recovery of companion metals can enhance overall profitability. However, only a small fraction of e-waste contains germanium, and the materials are often embedded in complex assemblies. Disassembly, sorting, and pre-concentration are labor-intensive and require sophisticated infrastructure. Furthermore, the volume of recoverable germanium from bulk e-waste streams is low, making large-scale operations economically challenging unless highly targeted. The technologies required for germanium extraction from e-waste, including selective leaching or vacuum smelting, are often capital-intensive and not yet widely implemented. Accordingly, germanium recovery from e-waste is economically viable primarily under selective, high-concentration scenarios rather than as a general strategy. In summary, e-waste offers significant potential in niche applications but remains economically constrained on a large scale. The development of a sustainable, long-term model for Ge supply must account for these realities while aligning with broader environmental objectives, as discussed in the next section.

5. Long-term sustainability model based on secondary supply of germanium from waste materials

Aligned with the EU's long-term sustainability vision,[181] the European Green Deal highlights the need to secure access to critical raw materials essential for a clean energy future.[182] A major challenge in germanium production is its recovery as a by-product. For instance, while zinc mining drives its own economic value, approximately 75% of global germanium production originates from ZRR waste.[183] Meanwhile, the amount of germanium contained in anthropogenic urban mines has been steadily increasing and is projected to continue rising until 2040 (Fig. 9a–f). With total scrap accumulation expected to reach over two thousand tons, the prediction model suggests that the largest share of Ge scrap (*i.e.*, 61%) comes from IR optics, where accumulation is expected to grow exponentially.[171] Additionally, the demand for germanium in solar cells is anticipated to accelerate significantly from 2035 in pursuit of a carbon-neutral future. Meeting this rising demand will require a corresponding increase in primary Ge production, projected through linear regression analysis of historical data from 2000 to 2020. Fig. 9g shows that the primary production of germanium is expected to reach above 140 t by 2040. This trend aligns with other sector-specific simulations of germanium demand and supply, which indicate an impending shortage (refer to Fig. 9i).[184] In this figure, the thin lines represent demand across various sectors, while the thick lines depict actual supply, revealing that all sectors except IR sensors are likely to face supply deficits. Consequently, a sharp increase in germanium price is anticipated around 2040, particularly if demand growth outpaces copper and zinc mining rates.

Recycling post-consumer electronic waste could mitigate this scarcity, but current recycling rates remain low (below 10%). Sverdrup and Haraldsson[184] presented a value chain linking the extraction of mother metals to germanium circulation (Fig. 10), highlighting the market dynamics and policy impacts described in the EEA's four sustainability scenarios.[181] These scenarios provide distinct policy pathways. The analysis indicates that Ecotopia focuses on conservation, minimal use, and a cooperative regulatory approach to reduce demand (represented by the R1 loop), whereas Unity in Adversity and Technocracy for Good focus more on centralized control, with the latter particularly focusing on technological solutions for efficient germanium circularity, reducing extraction *via* recycling (represented by the R2 loop). The analysis also suggests that physical circularity of germanium is critical to offset its primary supply. Understanding and improving recycling rates over time will align policy processes with feedback loops related to circularity. Moreover, economic and geopolitical factors often favor mother metal extraction, as shown by loops R3 and R4 in Fig. 10. Therefore, recognizing the driving forces behind extraction and their influence on market mechanisms is essential for ensuring long-term circularity of this critical metal.

6. Conclusions and future perspectives

Germanium has found widespread applications in electronics such as semi-conductors, diodes, and transistors, while its usage in fiber optics is currently soaring for high-speed internet and data transfer services. With no independent mineral deposits of germanium, its extraction as a by-product of zinc from sphalerite and through the processing of coal fly ash has attracted researchers worldwide to develop efficient methods for recovering this critical element. Over the past two decades, research efforts have also intensified to develop effective schemes for recycling germanium from various waste

materials, further contributing to its sustainable utilization and reducing dependence on co-existing primary sources. Ge extraction from industrial residues is primarily governed by its concentration in the parent material and the thermal and chemical transformations it undergoes during ore roasting or coal combustion. The resulting GeO_2 serves as the key leachable species, whose solubility and speciation in solution are highly pH-dependent. Acidic leaching using H_2SO_4 or HCl remains the dominant method, with HCl being particularly effective in silicate-rich matrices due to its ability to form $GeCl_4$, which can be purified *via* distillation or directly reduced to metallic germanium.

Efficient pre-concentration of germanium is critical for downstream recovery and can be achieved through tannin precipitation, solvent extraction, ion exchange, and adsorption, each requiring high selectivity over competing metals like zinc, iron, and cadmium. The success of these methods depends on factors such as pH, extractant compatibility, and system stability. Due to poor selectivity, high reagent consumption, emulsification issues, and thermal instability, the use of tannin-based precipitation processes has been largely phased out. Despite rapid mass transport rates, solvent extraction with synergistic systems like YW100 with D2EHPA and N235 has shown promising results, though third-phase formation, high cost of organic solvents, and co-extraction of metal ions are unresolved issues. Manoeuvring new extractants with higher selectivity and lower cost can offer a potential solution to this challenge. Solid-phase approaches using catechol and functionalized resins like Amberlite IRA-900 have demonstrated selectivity for germanium, offering additional potential for integration with solvent extraction to enhance overall yields. In recycling, up to 30% of germanium used in semiconductors could be recovered from waste streams, though challenges persist in liberating germanium from siliceous matrices, often requiring hydrofluoric acid or alkali roasting. Ionic liquids, particularly phosphonium-based variants in HCl media, show improved selectivity and could serve as greener alternatives. LCA studies reveal stark environmental differences among extraction pathways: the GWP for producing 1 kg of Ge from CBR with energy recovery is 698 kg CO_2-eq, which rises to 5566 kg CO_2-eq without energy integration, while ZRR-based production shows 852 kg CO_2-eq. In contrast, recycling from PV waste results in only 163 kg CO_2-eq, reinforcing the environmental benefits of targeted recycling. However, comprehensive data on the techno-economic and environmental performance of both conventional and emerging extraction technologies remain limited, especially at higher technology readiness levels. Bridging this gap is essential for establishing robust sustainability benchmarks and identifying critical process hotspots.

Future research on germanium should focus on developing efficient, low-cost, and environmentally friendly extraction and recycling technologies, particularly those capable of selectively recovering germanium from complex matrices in both industrial residues and e-waste. Advancements in solvent extraction, ion exchange, and hybrid separation systems, along with scalable process integration, are essential to improving recovery efficiency and economic viability. In parallel, exploring germanium's role in emerging technologies such as photonics, quantum computing, and energy storage will help to anticipate future demand and refine purity requirements. The anticipated growth in Ge-containing e-waste generation will also help to overcome the feedstock limitations. Comparative sustainability assessments, including processing costs and life-cycle impacts, should be expanded to establish robust benchmarks for different extraction routes. Moreover, policy research addressing circular economy incentives, recycling mandates, and extended producer responsibility (EPR) is crucial to strengthen regulatory frameworks for germanium recovery. A multidisciplinary approach combining technical innovation with economic and policy analysis will be key to securing a stable, sustainable supply of this critical element.

Overall, this review highlights the key points for achieving efficient germanium extraction and emphasizes the significance of adopting sustainable practices, particularly through the implementation of waste recycling strategies. By considering the environmental impacts of different production systems, stakeholders can make informed decisions and work towards a more sustainable metallurgical extraction of germanium.

Author contributions

R. R. Srivastava: conceptualization, methodology, visualization, writing – original draft, and writing – review & editing. S. Ilyas: conceptualization, methodology, visualization, writing – original draft, and writing – review & editing, funding acquisition, and supervision.

Conflicts of interest

There are no conflicts to declare.

Data availability

This review does not include primary research results, software, or code, and no new data were generated or analyzed as part of this work.

Supplementary information (SI): bibliometric data acquisition methods, Tables S1 and S2, highlighting key features of germanium leaching processes from different materials, and summarizing the solvent extraction papers reported in the literature, respectively. Table S3 summarizing the midpoint impact category determined *via* the LCA study on production of 1 kg of Ge. See DOI: https://doi.org/10.1039/d5gc03018h.

Acknowledgements

This work was supported by the Wallenberg Initiative Materials Science for Sustainability (WISE) funded by the Knut

and Alice Wallenberg Foundation. The authors greatly acknowledge WISE for its support within the thematic research area of *Circularity and Replacement*.

References

1 H. Tang, Y. Fu, B. Liu, L. Li, Z. Zhang, L. Wang and F. Jiang, *Sep. Purif. Technol.*, 2025, **365**, 132650.
2 Q. Tian, D. Wei, Y. Pan and H. Zhang, *Environ. Sci. Pollut. Res.*, 2024, **31**, 18485–18493.
3 J. Emsley, *Nature's Building Blocks: An A-Z Guide to the Elements*, Oxford University Press, New York, 2011.
4 N. Na, Y.-C. Lu, Y.-H. Liu, P.-W. Chen, Y.-C. Lai, Y.-R. Lin, C.-C. Lin, T. Shia, C.-H. Cheng and S. L. Chen, *Nature*, 2023, **627**, 295–300.
5 (*a*) Germanium (https://www.rsc.org/periodic-table/element/32/Germanium, accessed on 26th April 2025) (*b*) Germanium Ge (https://www.crystran.co.uk/optical-materials/germanium-ge, assessed on 24th April 2025).
6 W. J. Kim, V. Soshnikova, J. Markus, *et al.*, *Optik*, 2019, **178**, 664–668.
7 M. Ordu and S. N. Basu, *Infrared Phys. Technol.*, 2020, **111**, 103507.
8 P. C. Palleti, P. Seyidov, A. Gybin, *et al.*, *J. Mater. Sci.: Mater. Electron.*, 2024, **35**, 57.
9 V. Fthenakis, W. Wang and H. C. Kim, *Renewable Sustainable Energy Rev.*, 2009, **13**, 493–517.
10 V. Fthenakis, *Renewable Sustainable Energy Rev.*, 2009, **13**, 2746–2750.
11 R. P. de Oliveira, J. Benvenuti and D. C. R. Espinosa, *Renewable Sustainable Energy Rev.*, 2021, **145**, 111090.
12 X. Hu, C. Wang and A. Elshkaki, *Renewable Sustainable Energy Rev.*, 2024, **192**, 114217.
13 A. A. Valero, A. A. Valero, G. Calvo and A. Ortego, *Renewable Sustainable Energy Rev.*, 2018, **93**, 178–200.
14 A. A. Khan, M. Noman and S. T. Jan, *Opt. Quantum Electron.*, 2025, **57**, 114.
15 H. K. Haghighi and M. Irannajad, *Environ. Sci. Pollut. Res.*, 2022, **29**, 48126–48151.
16 R. Holl, M. Kling and E. Schroll, *Ore Geol. Rev.*, 2007, **30**, 145–180.
17 R. R. Moskalyk, *Miner. Eng.*, 2004, **17**(3), 393–402.
18 J. Wang and A. He, *Modern Germanium Metallurgy*, Metallurgical Industry Press, Beijing, 2005.
19 M. Patel and A. K. Karamalidis, *Sep. Purif. Technol.*, 2021, **275**, 118981.
20 Mineral Commodity Summaries, USGS 2020 (https://www.usgs.gov/data/germanium-deposits-united-states, assessed on 12th April 2025).
21 D. C. Curtolo, S. Friedrich and B. Friedrich, *J. Cryst. Process Technol.*, 2017, **7**, 65–84.
22 U.S. Geological, Survey Releases 2022, List of Critical Minerals (https://www.usgs.gov/news/national-news-release/us-geological-survey-releases-2022-list-critical-minerals, assessed on 22th April 2025).
23 Study on the critical raw materials for the EU 2023 (https://op.Europa.eu/en/publication-detail/-/publication/57318397-fdd4-11ed-a05c-01aa75ed71a1, assessed on 25th April 2025).
24 E. Righetti and V. Rizos, *Intereconomics*, 2023, **58**(2), 69–73.
25 Critical raw materials (https://single-market-economy.ec.Europa.eu/sectors/raw-materials/areas-specific-interest/critical-raw-materials_en, accessed on 18th March 2025).
26 J. Tao, Z. Tao and L. Zhihong, *J. Cleaner Prod.*, 2021, **294**, 126217.
27 O. Kwon and I. Sohn, *Resour., Conserv. Recycl.*, 2020, **158**, 104809.
28 X. Lin, Z. Peng, J. Yan, Z. Li, J. Hwang, Y. Zhang, G. Li and T. Jiang, *J. Cleaner Prod.*, 2017, **149**, 1079–1100.
29 J. Wang, Y. Zhang, K. Cui, T. Fu and T. Algarni, *J. Cleaner Prod.*, 2021, **298**, 126788.
30 D. Liang, J. Wang, Y. Wang, F. Wang and J. Jiang, *Hydrometallurgy*, 2008, **93**, 140–142.
31 D. Liang, J. Wang and Y. Wang, *Hydrometallurgy*, 2009, **95**, 5–7.
32 F. Arroyo, O. Font, C. Fernandez-Pereira, X. Querol, R. Juan, C. Ruiz and P. Coca, *J. Hazard. Mater.*, 2009, **167**(1–3), 582–588.
33 F. A. Torralvo and C. Fernandez-Pereira, *Miner. Eng.*, 2011, **24**(1), 35–41.
34 F. Liu, Z. Liu, Y. Li, *et al.*, *Hydrometallurgy*, 2017, **171**, 149–156.
35 H. Wang, L. Jiangshun, J. Kaixi and Q. Dingfan, Recovery of Ga, Ge from zinc residues by hydrometallurgical processes, in *International Symposium of Advanced Processing of Metals and Materials Proceeding*, California (USA), 2006, vol. 7, pp. 413–420.
36 T. Zhang, T. Jiang and Z. Liu, *Miner. Eng.*, 2019, **136**, 155–160.
37 Germanium - The Hidden Treasure from Recycling Scrap Germanium Materials, ORYXMETALS (https://www.oryx-metals.com/post/germanium-the-hidden-treasure-from-recycling-germanium-materials, accessed on 23rd March 2025).
38 O. N. Kolesnik, A. N. Kolesnik, V. T. S″edin, *et al.*, *Dokl. Earth Sci.*, 2024, **519**, 2313–2319.
39 I. G. Dedovets, *Coke Chem.*, 2025, **68**, 407–410.
40 M. Filella, *Environ. Sci. Pollut. Res.*, 2022, **29**, 65873–65874.
41 M. Filella, *Environ. Sci. Pollut. Res.*, 2022, **29**, 65875.
42 P. Meshram and Abhilash, *Min., Metall., Explor.*, 2022, **39**, 689–707.
43 T. H. Nguyen and M. S. Lee, *Miner. Process. Extr. Metall. Rev.*, 2021, **42**(6), 406–426.
44 The 17 Goals, United Nations Department of Economic and Social Affairs (https://www.rsc.org/periodic-table/element/32/Germanium, assessed on 22nd April 2025).
45 C. H. Liu, A. S. Pashinkin and A. V. Novoselova, *Dokl. Akad. Nauk SSSR*, 1963, **151**, 1335–1338.
46 C. Licht, L. T. Peiro and G. Villalba, *J. Ind. Ecol.*, 2015, **19**(5), 890–903.

47 R. Mu, S. Wang, X. Wang, Y. Zhao and Z. Dong, *ACS Omega*, 2023, **8**(19), 17264–17273.
48 F. Arroyo and C. Fernandez-Pereira, *Ind. Eng. Chem. Res.*, 2008, **47**(9), 3186–3191.
49 A. S. Yakushevich, S. Y. Bratskaya, V. V. Ivanov, N. V. Polyakova and V. A. Avramenko, *Geochem. Int.*, 2013, **51**, 405–412.
50 W. Chen, *Yunan Metall.*, 1991, 8–44.
51 O. Font, X. Querol, F. E. Huggins, *et al.*, *Fuel*, 2005, **84**(11), 1364–1371.
52 O. Font, X. Querol, A. Lopezsoler, *et al.*, *Fuel*, 2005, **84**(11), 1384–1392.
53 X. Liu, C. Zheng, Z. Miao, E. Xu, Y. Han and L. Ding, *Sep. Purif. Technol.*, 2025, **354**(3), 128915.
54 X. Dong, Z. Shuai, H. Tao, *et al.*, *Clean Coal Technol.*, 2023, **29**(4), 13–20.
55 O. H. Johnson, *Chem. Rev.*, 1952, **51**(3), 431–469.
56 M. Micoulaut, L. Cormier and G. S. Henderson, *J. Phys.: Condens. Matter*, 2006, **18**(45), R753.
57 T. Sasamoto, M. Kobayashi and T. Sata, *J. Mass Spectrom. Soc. Jpn.*, 1981, **29**(3), 249–255.
58 G. S. Pokrovski and J. Schott, *Geochim. Cosmochim. Acta.*, 1998, **62**(9), 1631–1642.
59 J. H. Müller, *Proc. Am. Philos. Soc.*, 1926, **65**, 183–195.
60 T. B. Kosova, L. N. Dem'yanets and T. G. Uvarova, *Russ. J. Inorg. Chem.*, 1987, **32**, 430–432.
61 V. A. Vehov, B. S. Birtuhnovskaya and R. F. Doronkina, *Izv. Vusov. Khim. Khim. Tekhnol.*, 1964, **7**, 1018–1019.
62 R. Schwartz and E. Huf, *Z. Anorg. Allg. Chem.*, 1931, **203**, 188–218.
63 H. Park and L. L. Tavlarides, *Ind. Eng. Chem. Res.*, 2019, **48**(8), 4014–4021.
64 S. A. Wood and I. M. Samson, *Ore Geol. Rev.*, 2006, **28**, 57–102.
65 G. Cote and D. Bauer, *Hydrometallurgy*, 1980, **5**(2–3), 149–160.
66 B. Marchon, G. Cote and D. Bauer, *J. Inorg. Nucl. Chem.*, 1979, **41**, 1353–1363.
67 V. A. Nazarenko, in *Analytical Chemistry of Germanium*, Wiley, Chichester, 1974, pp. 23–25.
68 L. R. Bernstein and G. A. Waychunas, *Geochim. Cosmochim. Acta.*, 1987, **51**(3), 623–630.
69 E. G. Rochow, Germanium, in *The Chemistry of Germanium, tin and lead*, ed. E. W. Abel, Pergamon Press, Oxford, 1973, pp. 1–41.
70 B. Gupta and N. Mudhar, *Sep. Sci. Technol.*, 2006, **41**(3), 549–572.
71 M. Kul and Y. Topkaya, *Hydrometallurgy*, 2008, **92**, 87–94.
72 J. E. Dutrizac, T. T. Chen and R. J. Longton, *Metall. Mater. Trans. B*, 1996, **27**, 567–576.
73 M. P. Wardell and C. F. Davidson, *JOM*, 1987, **39**, 39–41.
74 D. D. Harbuck, J. C. Judd and D. V. Behunin, *Solvent Extr. Ion Exch.*, 1991, **9**, 383–401.
75 D. D. Harbuck, *Gallium and germanium recovery from domestic sources*, US Department of the Interior, Bureau of Mines, 1992.
76 T. Jiang, T. Zhang, F. Ye and Z. Liu, *Miner. Eng.*, 2019, **137**, 334–343.
77 F. Liu, Z. Liu, Y. Li, Z. Liu, Q. Li and L. Zeng, *Hydrometallurgy*, 2016, **164**, 313–320.
78 M. Drzazga, R. Prajsnar, A. Chmielarz, *et al.*, *Metals*, 2018, **8**, 1041.
79 A. E. Torma and H. Jiang, *Miner. Process. Extr. Metall. Rev.*, 1991, **7**(3–4), 235–258.
80 J. E. Hoffmann, *JOM*, 1987, **39**(6), 42–45.
81 A. V. Vorotyntsev, V. M. Vorotyntsev, A. N. Petukhov, *et al.*, *Inorg. Mater.*, 2016, **52**, 919–924.
82 A. V. Kadomtseva, A. M. Ob"edkov and M. A. Zasovskaya, *Inorg. Mater.*, 2020, **56**, 229–234.
83 A. V. Kadomtseva and A. M. Ob"edkov, *Inorg. Mater.*, 2017, **53**(12), 1312–1318.
84 R. Kornev, I. Gornushkin, L. Shabarova, *et al.*, *Science*, 2024, **6**(1), 1.
85 F. Liu, Z. Liu, Y. Li, B. P. Wilson and M. Lundström, *Int. J. Miner. Process.*, 2017, **163**, 14–23.
86 J. Song, C. Peng, Y. Liang, *et al.*, *Hydrometallurgy*, 2021, **202**, 105599.
87 D. A. Everest, *J. Chem. Soc.*, 1955, **84**(18), 4415–4418.
88 F. Liu, Z. Liu, Y. Li, B. P. Wilson and M. Lundström, *Hydrometallurgy*, 2017, **169**, 564–570.
89 H. Di, Q. Gui, F. Yang, *et al.*, *Chem. Eng. Process.*, 2021, **161**, 108293.
90 L. Zhang, W. Guo, J. Peng, *et al.*, *Ultrason. Sonochem.*, 2016, **31**, 143–149.
91 S. Rao, D. Wang, Z. Liu, *et al.*, *Hydrometallurgy*, 2019, **183**, 38–44.
92 L. A. Admakin, *Coke Chem.*, 2019, **62**(10), 437–446.
93 D. Makowska, F. Wierońska, A. Strugala and K. Kosowska, *E3S Web Conf.*, 2016, **10**, 00121.
94 Q. Wei and S. M. Rimmer, *China Int. J. Coal Geol.*, 2017, **178**, 39–55.
95 F. Vejahati, Z. Xu and R. Gupta, *Fuel*, 2010, **89**, 904–911.
96 Y. Sun, G. Qi, X. Lei, *et al.*, *J. Environ. Sci.*, 2016, **43**, 91–98.
97 S. Dai, V. V. Seredin, C. R. Ward, *et al.*, *Int. J. Coal Geol.*, 2014, **121**, 79–97.
98 S. Dai and R. B. Finkelman, *Int. J. Coal Geol.*, 2018, **186**, 155–164.
99 R. Yang, W. Song, S. Rao, *et al.*, *Materials*, 2023, **16**, 5374.
100 J. M. Chimenos, A. I. Fernández, R. del Valle-Zermeño, *et al.*, *Fuel*, 2013, **112**, 450–458.
101 F. Arroyo, O. Font, J. M. Chimenos, *et al.*, *Fuel Process. Technol.*, 2014, **124**, 222–227.
102 D. Guberman, *Earth*, 2010, **55**(5), 27.
103 P. Rafiee, S. Ghassa, F. Moosakazemi, *et al.*, *J. Cleaner Prod.*, 2021, **315**, 128223.
104 E. Rosenberg, *Rev. Environ. Sci. Bio/Technol.*, 2009, **8**(1), 29–57.
105 S. Dhiman and B. Gupta, *J. Environ. Manage.*, 2020, **276**, 111218.
106 W. S. S. Chen, B. C. C. Chang and K. L. L. Chiu, *J. Environ. Chem. Eng.*, 2017, **5**, 5215–5221.
107 D. D. Harbuck, *Miner. Metall. Process.*, 1993, **10**, 1–4.

108 W. S. Chen, B. C. Chang and Y. J. Chen, *IOP Conf. Ser.: Earth Environ. Sci.*, 2018, **159**, 012008.
109 W. S. Chen, B. C. Chang and C. K. Shuai, *IOP Conf. Ser.: Earth Environ. Sci.*, 2020, **720**, 012005.
110 S. Y. Lee, M. Lee, S. Lee, S. S. Cho and M. Seo, *Mater. Test.*, 2018, **60**(4), 413–417.
111 K. Kuroiwa, S. I. Ohura, S. Morisada, *et al.*, *Miner. Eng.*, 2014, **55**, 181–185.
112 W. Wang, F. Wang and F. Lu, *Metall. Res. Technol.*, 2018, **115**(2), 203.
113 F. A. Torralvo and Ferńandez-Pereira, *Miner. Eng.*, 2011, **24**(1), 35–41.
114 F. A. Arroyo, C. Ferńandez-Pereira, E. G. Villard, Y. Luna, C. Leiva, L. Vilches and R. Villegas, *Miner. Eng.*, 2018, **128**, 106–114.
115 P. Dytrych, J. Bumba, F. Kastanek, *et al.*, *Ind. Eng. Chem. Res.*, 2017, **56**, 12863–12869.
116 J. Bumba, P. Dytrych, R. Fajgar, *et al.*, *Ind. Eng. Chem. Res.*, 2018, **57**, 8855–8862.
117 L. Zhang, Q. Song and Z. Xu, *ACS Sustainable Chem. Eng.*, 2019, **7**(2), 2176–2186.
118 Q. Song, L. Zhang and Z. Xu, *J. Cleaner Prod.*, 2019, **207**, 522–530.
119 W. Qin, Y. Liu and C. Yanhong, *et al.*, *Chinese Pat*, 2014, 102951618A.
120 H. Akaike, *Japanese Pat*, 2015105226A, 2017.
121 S. Chao, *Chinese Pat*, 115821074B, 2025.
122 S. Xu, Z. Lu, X. Li, *et al.*, *Environ. Chem. Lett.*, 2025, **23**, 1341–1379.
123 F. Yang, M. Liang, H. Di, K. Yang and L. Zhang, *J. Kunming Univ. Sci. Technol. (Nat. Sci. Ed.)*, 2021, **46**, 9–17.
124 J. Cho, S. Roy, A. Sathyapalan, L. M. Free and Z. Z. Fang, *J. Powder Metall. Min.*, 2017, **6**(3), 1000183.
125 K. Liu, Y. Hong, J. Dai, *et al.*, *Arabian J. Chem.*, 2025, **18**, 2882024.
126 Y. Hong, H. Di, S. Li, K. Yang and L. Zhang, *Metals*, 2023, **13**(4), 774.
127 S. Bayat, S. Aghazadeh, M. Noaparast, M. Gharabaghi and B. Taheri, *J. Cent. South Univ.*, 2016, **23**, 2214–2222.
128 C. Xiong, *Yunnan Metall.*, 2009, **38**, 78–81.
129 Y. Li, W. Fu and J. Liu, *Yunnan Metall.*, 2021, **50**(2), 47–50.
130 M. Drzazga, A. Chmielarz, G. Benke, *et al.*, *Appl. Sci.*, 2019, **9**(5), 966.
131 P. Schofield, D. M. Mbugua and A. N. Pell, *Anim. Feed Sci. Technol.*, 2021, **91**(1), 21–40.
132 R. R. Srivastava, J.-c. Lee and M.-S. Kim, *J. Chem. Technol. Biotechnol.*, 2015, **90**(19), 1752–1764.
133 X. Ma, W. Qin and X. Wu, *J. Cent. South Univ.*, 2013, **20**, 1978–1984.
134 R. A. Kumbasar, *Hydrometallurgy*, 2009, **95**(3–4), 290–296.
135 S. Willersinn and H. Bart, *Int. J. Chem. Kinet.*, 2016, **48**(10), 609–621.
136 H. K. Haghighi, M. Irannajad and D. Moradkhani, *Physicochem. Probl. Miner. Process.*, 2019, **55**(1), 225–236.
137 A. de Schepper, *Hydrometallurgy*, 1976, **1**(3), 291–298.
138 D. H. Longsdail and M. J. Slater, *Solvent Extraction in the Process Industries, ISEC 93*, Springer, Dordrecht, 1993.
139 S. Nusen, Z. W. Zhu, T. Chairuangsri and C. Y. Cheng, *Hydrometallurgy*, 2015, **151**, 122–132.
140 S. Nusen, T. Chairuangsri, Z. W. Zhu and C. Y. Cheng, *Hydrometallurgy*, 2016, **160**, 137–146.
141 D. A. D. Boateng, D. A. Neudorf and V. N. Saleh, *US Pat*, 4915919A, 1990.
142 A. D. Schepper, M. Coussement and A. V. Peteghem, *US Pat*, 4432952A, 1984.
143 Z. Tan, Y. Zhen, C. Wei, *et al.*, *Sep. Purif. Technol.*, 2024, **329**, 125175.
144 I. Y. Fleitlikh, N. A. Grigorieva and O. A. Logutenko, *ChemistrySelect*, 2021, **6**(17), 4285–4291.
145 S. Tang, C. Zhou, X. Jiang and C. Zhao, *J. Cent. South Univ. Technol.*, 2000, **7**, 40–42.
146 Z. Lingzhi, T. Runchang and Z. Jiangyan, *Chin. J. Rare Met.*, 1981, **6**, 7–14.
147 B. M. Sargar and M. A. Anuse, *J. Anal. Chem.*, 2005, **60**, 404–408.
148 W. Vereycken, M. D. Belder, S. Riaño, T. V. Gerven and K. Binnemans, *Ind. Eng. Chem. Res.*, 2022, **61**, 5295–5305.
149 H. K. Haghighi, M. Irannajad, A. Fortuny and A. M. Sastre, *Hydrometallurgy*, 2018, **175**, 164–169.
150 M. Drzazga, M. Chmielarz, S. Kozlowicz and S. Kasierot, *Miner. Eng.*, 2024, **218**, 108984.
151 T. Zhang, T. Jiang and Z. Liu, *Miner. Eng.*, 2021, **160**, 106682.
152 M. Drzazga, A. Palmowski, G. Benke, M. Chmielarz, *et al.*, *Hydrometallurgy*, 2021, **202**, 105605.
153 D. R. E. Bauer, G. Cote, P. Fossi and B. Marchon, US4389379A, 1983.
154 T. Zhou, X. Zhong and L. Zheng, *JOM*, 1989, **41**, 36–40.
155 J. H. Vliegen, G. G. Haesebroek and A. J. De Schepper, WO1990013677A1, 1990.
156 J. H. Vliegen, G. G. Haesebroek and A. J. De Schepper, US5277882A, 1994.
157 V. Vojković, I. Juranović and B. Tamhina, *Croat. Chem. Acta*, 2001, **74**, 467–477.
158 S. Virolainen, J. Heinonen and E. Paatero, *Sep. Purif. Technol.*, 2013, **104**, 193–199.
159 S. Yasuda and K. Kawazu, *Sep. Sci. Technol.*, 1991, **26**, 1273–1277.
160 Y. Inukai, Y. Kaida and S. Yasuda, *Anal. Chim. Acta*, 1997, **343**, 275–279.
161 C. A. Cruz, S. Marie, G. Arrachart, *et al.*, *Sep. Purif. Technol.*, 2018, **193**, 214–219.
162 Y. Inukai, Y. Tanaka, Y. Shiraishi, *et al.*, *Anal. Sci.*, 2001, **17icas**, i1117–i1120.
163 H. Takemura, S. Morisada, K. Ohto, *et al.*, *J. Chem. Technol. Biotechnol.*, 2013, **88**(8), 1468–1472.
164 F. A. Torralvo, C. Fernández-Pereira and M. C. Campanario, *Ind. Eng. Chem. Res.*, 2010, **49**(10), 4817–4823.
165 A. Nozoe, K. Ohto and H. Kawakita, *Sep. Sci. Technol.*, 2012, **47**(1), 62–65.

166 C. He, M. Qi, Y. Liu, Z. Liu, Y. Wei, T. Fujita, G. Wang, S. Ma, W. Yang and J. Gan, *Hydrometallurgy*, 2024, **224**, 106230.
167 M. Patel and A. K. Karamalidis, *Chem. Eng. J.*, 2023, **475**, 146367.
168 J. P. Marco-Lozar, D. Cazorla-Amorós and A. Linares-Solano, *Carbon*, 2007, **45**(13), 2519–2528.
169 J. P. Marco-Lozar, A. Linares-Solano and D. Cazorla-Amorós, *Carbon*, 2011, **49**(10), 3325–3331.
170 H. Xiang, F. Zhao, T. Wun, *et al.*, *Sep. Purif. Technol.*, 2023, **311**, 123338.
171 M. Wong, J. Li and X. Zeng, *Front. Environ. Sci. Eng.*, 2025, **19**, 25.
172 T. Zimmermann and S. Gößling-Reisemann, *Resources*, 2014, **3**(1), 291–318.
173 F. Melcher and P. Buchholz, in *Germanium, Critical Metals Handbook*, John Wiley & Sons Ltd, Hoboken (NJ, USA), 2013, pp. 177–203.
174 B. Kumar, R. R. Srivastava and S. P. Barik, *Miner. Eng.*, 2023, **202**, 108289.
175 Y. Pujara, J. Govani, H. T. Patel, *et al.*, *Environ. Adv.*, 2023, **12**, 100364.
176 R. R. Srivastava, G. Nandikesh, S. Ilyas, P. Pathak and D. K. Rajak, *Sci. Total Environ.*, 2024, **929**, 172657.
177 B. Robertz, J. Verhelle and M. Schurmans, *JOM*, 2015, **67**, 412–424.
178 G. V. Hoof, M. Schurmans, B. Robertz, J. Menard and K. Dessein, *J. Sustain. Metall.*, 2020, **6**, 333–343.
179 ILCD guidance document, European Commission—Joint Research Centre—Institute for Environment and Sustainability International Reference Life Cycle Data System (ILCD) Handbook—General guide for Life Cycle Assessment—Detailed guidance, in *EUR 24708 EN*, Publications Office of the European Union, Luxembourg, 1st edn, 2010.
180 A. Ciroth, *Int. J. Life Cycle Assess.*, 2007, **12**, 209–210.
181 . European Environment Agency. Imaging a sustainable Europe in 2050. (https://www.eea.europa.eu/en/analysis/publications/imagining-a-sustainable-europe-in-2050, accessed on 12th May 2025).
182 H. U. Sverdrup, O. van Allen and H. V. Haraldsson, Modelling indium extraction, supply, price, use and recycling 1930–2200 using the WORLD7 model; implication for the imaginaries of Sustainable Europe 2050, in *Natural resources research*, Springer, Berlin, 2024.
183 . United States Geological Survey. Commodity statistics for a number of metals (consulted several times 2008–2024). Available at: https://minerals.usgs.gov/minerals/pubs/commodity/(assessed on 12th May 2025).
184 H. U. Sverdrup and H. V. Haraldsson, *Biophys. Econ. Sust.*, 2024, **9**, 5.

